

RICE UNIVERSITY

**Engineering Adeno-Associated Virus for Protease-Targeted Gene Therapy and  
Immune Avoidance**

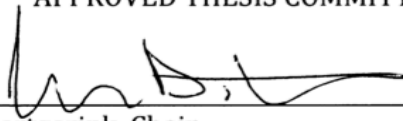
by

**Tawana Michelle Robinson**

A THESIS SUBMITTED  
IN PARTIAL FULFILLMENT  
OF THE REQUIREMENTS FOR THE DEGREE

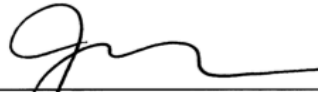
**Doctor of Philosophy**

APPROVED THESIS COMMITTEE:



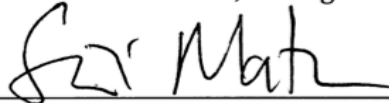
---

Jeffrey Hartgerink, Chair  
Professor, Chemistry and Bioengineering



---

Junghae Suh  
Associate Professor, Bioengineering



---

Dean Seichi Matsuda  
E. Dell Butcher Chair in Chemistry  
Professor of Chemistry and Biochemistry & Cell Biology



---

K. Jane Grande-Allen  
Isabel C. Cameron Professor  
Chair, Bioengineering

Houston, TX  
May 2019

# **ABSTRACT**

## **Engineering Adeno-Associated Virus for Protease Targeted Gene Therapy and Immune Avoidance**

by

**Tawana Michelle Robinson**

Adeno-associated virus (AAV) has earned significant attention as a safe and efficient gene therapy tool. AAV has been used in over 100 clinical trials to treat a variety of human diseases. However, non-specific targeting to diseased cells and activation of the host immune response hinder its therapeutic efficacy. To address these challenges, genetic modification of the AAV capsid can lead to an improved gene delivery platform. Therefore, capsid-engineering strategies may be necessary to develop optimized vectors for clinical progress.

This present work reveals design rules governed by amino acid properties for engineered AAV to become activated by upregulated proteolytic biomarkers in diseased sites. AAV constructs with varying chemical properties were synthesized and characterized for functional behavior. In parallel, a Nature-inspired strategy was employed to create an immune-evasive AAV vector. A

panel of AAV vectors with inserted stealth peptides in the AAV capsid was generated to study immune cell uptake. Finally, to gain a better understanding of AAV intracellular trafficking, we found several amino acid residues that are necessary for viral infectivity. The ultimate goal for my research contributions is to develop and to advance AAV vectors for future clinical applications.

## **Acknowledgments**

First, I will like to thank Junghae Suh for your mentorship in shaping me to become a scientist. I am grateful for you pushing me to prepare me for the future that you envisioned for me - towards academic leadership and a stellar research career. Thank you for always coaching me and allowing me to pursue my research passion.

Thank you Jeffrey Hartgerink for your guidance and scientific advice throughout the years. Your dedication in supporting my research goals during challenging circumstances is unforgettable.

Thank you Dean Matsuda for your endless support, advice, and guidance. You have inspired me to pursue excellent research, but also the importance of being involved in serving others in the Rice community.

Thank you Jane Grande-Allen for mentoring me and being a supportive anchor throughout my predoctoral career. You made tremendous efforts to be available for me to talk about my research and career opportunities.

Finally, I give a special thank you to all of my friends and family who fed me, supported me, and loved me endlessly through such a challenging journey.

# Table of Contents

<b>Chapter 1: Introduction.....</b>	<b>2</b>
Gene Therapy.....	2
Adeno-Associated Virus (AAV).....	4
<i>AAV Structure and Genome.....</i>	<i>4</i>
<i>AAV Intracellular Trafficking.....</i>	<i>5</i>
<i>AAV Immune Response.....</i>	<i>7</i>
<i>AAV Transgene Immune Response.....</i>	<i>7</i>
<i>AAV Capsid Immune Response.....</i>	<i>8</i>
AAV Capsid Engineering.....	9
<i>Rational insertion of defined peptide/protein.....</i>	<i>10</i>
<i>Rational insertion of random peptide.....</i>	<i>12</i>
<i>Random insertion of defined peptide/protein.....</i>	<i>13</i>
<i>Tweaking viruses through point mutations.....</i>	<i>15</i>
<i>Random point mutations.....</i>	<i>15</i>
<i>Rational point mutations.....</i>	<i>16</i>

Thesis Overview.....	17
<b>Chapter 2: Role of Tetra Amino Acid Motif Properties on the Function of Protease-Activatable Viral Vectors.....</b>	<b>22</b>
Introduction.....	22
Results.....	24
<i>Production of Viruses with Peptide Lock Variants.....</i>	24
<i>Capsid Stability of Viruses with Peptide Lock.....</i>	27
<i>Impact of Peptide Lock Variants on Heparin Binding.....</i>	28
<i>Ability of Peptide Lock Variants to Block Cellular Transduction.....</i>	29
<i>Ability of Peptide Locks to be Cleaved by Extracellular Proteases.....</i>	32
Discussion.....	34
Conclusions.....	37
Materials and Methods.....	39
References.....	44
<b>Chapter 3: Engineering Adeno-Associated Virus with a Self-Peptide for Immune Evasion.....</b>	<b>49</b>

Introduction.....	49
Results.....	51
<i>Synthesis of AAV-SP variants.....</i>	51
<i>Infectivity of AAV-SP variants.....</i>	53
<i>Phagocytic Susceptibility of AAV-SP variants.....</i>	54
Discussion and Conclusions.....	56
Materials and Methods.....	59
References.....	61

**Chapter 4: Investigation of an Essential Serine-Rich Motif for AAV Intracellular Trafficking to the Nucleus**

Introduction.....	67
Results.....	69
<i>Bioinformatic Alignment of N-Terminal S/T Motif in AAV VP1 and VP2 Subunits.....</i>	69
<i>Production of AAV2 Vectors with Alanine Substitutions in the N-Terminal S/T motif.....</i>	71
<i>Transduction Efficiency of AAV2 N-Terminal S/T Motif Mutants.....</i>	72

<i>Cellular Internalization of AAV2 N-Terminal S/T Motif</i>	
<i>Mutants</i> .....	74
<i>Nuclear Uptake of AAV2 N-Terminal S/T Motif</i>	
<i>Mutants</i> .....	74
<i>Nuclear Uncoating of AAV2 N-Terminal S/T Motif</i>	
<i>Mutants</i> .....	75
<i>Transcriptional Levels of AAV2 N-Terminal S/T Motif</i>	
<i>Mutants</i> .....	77
Discussion and Conclusions.....	77
Materials and Methods.....	80
References.....	86
<b>Chapter 5: Conclusions and Future Directions</b> .....	<b>94</b>

## List of Figures

Figure 1-1 Timeline for 50 years of AAV vector technology.....	3
Figure 1-2 AAV Structure and Genome .....	5
Figure 1-3 AAV Cellular Trafficking.....	6
Figure 2-1 Protease-activatable virus (provector) design and concept.....	23
Figure 2-2 Titers of provector candidates with different tetra amino acid (4AA) motifs.....	25
Figure 2-3 Detection of viral capsid proteins (VPs) and peptide lock incorporation of provector candidates via Western blot.....	26
Figure 2-4 Capsid stabilities of provector candidates as assessed by their abilities to protect their genomes from nuclease digestion.....	28
Figure 2-5 Ability of various 4AA motifs to disrupt virus-heparin binding.....	29
Figure 2-6 Transduction assay to test if the various 4AA motifs are able to inhibit cellular transduction by provector candidates in the absence of proteases.....	30
Figure 2-7 Detection of proteolyzed VP fragments of Provector-D4	

and Provector-E4 in the presence of MMP7.....	33
Figure 2-8 Recovery of cellular transduction ability of Provector-D4 and Provector-E4 in the presence of MMP7.....	34
Figure 3-1 Design of SP insertion into AAV capsid.....	51
Figure 3-2 Structural characterization of AAV-SP.....	52
Figure 3-3 Transduction of AAV-SP mutants.....	54
Figure 3-4 Macrophage uptake of AAV-SP mutants.....	55
Figure 3-5 Macrophage uptake of AAV-SP mutants with anti- SIRPa.....	56
Figure 4-1 Multiple sequence alignment of 167 AAV VP1 sequences.....	70
Figure 4-2 Production of AAV2 vectors with alanine substitutions in the N-terminal S/T motif.....	72
Figure 4-3 Transduction efficiencies of AAV2 S/T motif mutants in HeLa and HEK293T cells.....	73
Figure 4-4 Cellular uptake of AAV2 S/T motif mutants in HeLa cells.....	74
Figure 4-5 Nuclear uptake of AAV2 S/T motif mutants in HeLa cells.....	75

Figure 4-6 Nuclear capsid uncoating of AAV2 S/T motif mutants  
in HeLa cells..... 76

Figure 4-7 GFP mRNA expression levels of AAV2 S/T motif  
mutants..... 77

This page was intentionally left blank

# INTRODUCTION

## Gene Therapy

Gene therapy began almost fifty years ago as a treatment strategy for genetic human diseases (**Figure 1-1**)<sup>1</sup>. Initially conceived as a treatment solely for inherited diseases, gene therapy is now being applied to acquired conditions as well, such as genetic engineering of T cells for cancer immunotherapy. In the 1990s, gene therapy was tested in human clinical trials<sup>1</sup>. Unfortunately, one of the trials to deliver the ornithine transcarbamylase (OTC) gene via an adenoviral vector produced no therapeutic benefits and resulted in the unexpected death of Jesse Gelsinger<sup>2</sup>. One primary explanation for disappointing clinical results was insufficient knowledge of viral vector biology. Success was finally achieved for the gene therapy of an X-linked inherited form of severe combined immunodeficiency<sup>3</sup>. At least 90% of the patients were effectively treated for immunodeficiency<sup>4</sup>. For another hematopoietic disorder, chronic granulomatous disease (CGD), researchers observed clinical progress in diminished immune infections<sup>3</sup>. Efficient genetic modification of targeted cells was observed during these clinical investigations; however, research progress was hindered by various toxicities, e.g. insertional genotoxicity and immune responses<sup>1</sup>. Within this current decade, gene therapy has grown in overcoming safety concerns and improving gene delivery.

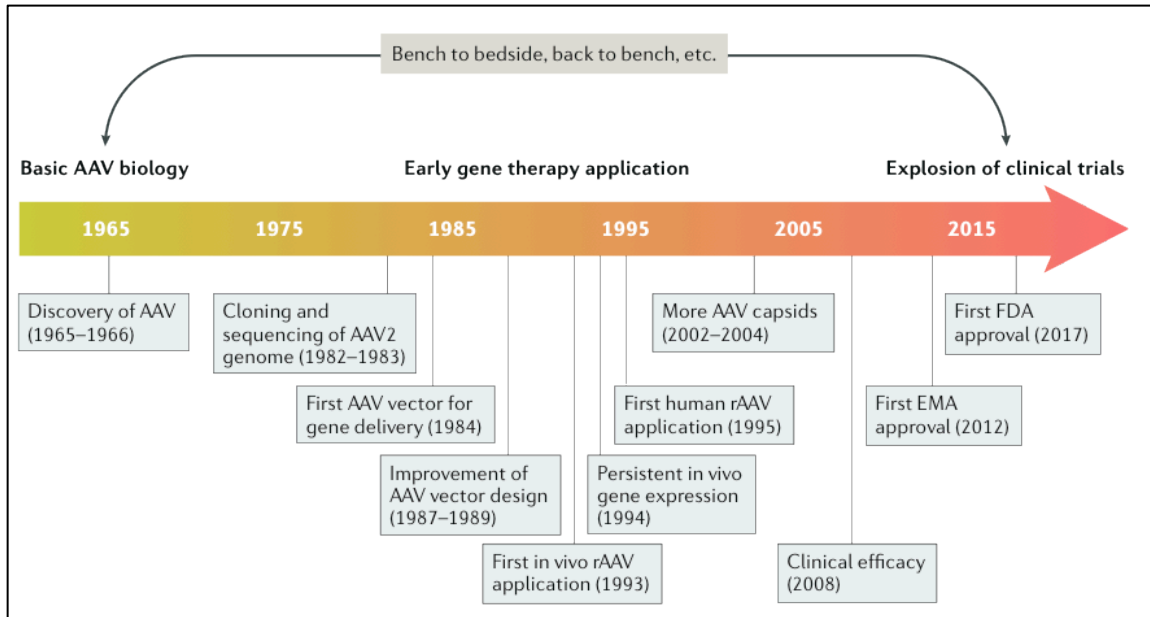


**Figure 1-1. Timeline for 50 years of AAV vector technology.** AAV was first discovered in 1965 and 1966. Over two decades, basic biology research enabled the genetic engineering of the AAV genome. In the late 1980s, AAV was developed for vector delivery, including vast improvements of its design. These vectors were then applied to *in vivo* models and to humans. For this current decade, AAV has reached significant achievement as an approved gene therapy product on the market.<sup>1</sup> Figure used with publisher's permission.

As a result, gene-based therapies have been approved for clinical use, in particular viral vectors. For instance, adeno-associated virus (AAV) has contributed to key clinical successes and has demonstrated clinical promise in the gene therapy field. In 2012, alipogene tiparvovec (Glybera), was authorized by the European Medicines Agency to be the first AAV gene therapy drug to treat lipoprotein lipase deficiency. Nearly five years later, voretigene neparvovec-rzyl (Luxturna) was approved as the first AAV gene therapy product in the United States<sup>5</sup>. Currently, AAV vectors are the leading platform in the gene therapy field.

## **Adeno-Associated Virus (AAV)**

AAV vectors are non-enveloped and replication-defective viruses that belong to the genus *Dependovirus* of the family Parvoviridae<sup>5</sup>. As a gene therapy vector, AAV offers advantages of being non-pathogenic; infects dividing and non-dividing cells with high efficiency; and displays low immunogenicity compared to other viral vectors. However, AAV vectors have several drawbacks: its limited DNA packaging (~5kb), anti-AAV immune responses, and non-specific gene delivery. All of these existing challenges continue to be a primary emphasis of research efforts to advance AAV for improved clinical efficiency. For successful strides in AAV vector technology, AAV biology must be further understood.

### *AAV Structure and Genome*

AAV is ~25 nm in diameter and contains a single-stranded DNA genome of ~4.7 kb. Its genome contains the *rep* and *cap* genes that are flanked by two-inverted terminal repeats (ITRs), which function as origins of replication and packaging signals (**Figure 1-2**). The *rep* gene encodes four non-structural proteins (Rep78, Rep68, Rep52 and Rep40) required for viral replication, capsid assembly, genome packaging, and integration. The promoters, p5 and p19, participate in *rep* gene product expression. The *cap* gene encodes three viral capsid subunit proteins (VPs) that form the icosahedral capsid. All three capsid subunits share a common VP3 structural domain. Expression of these VPs is done through alternative splicing and translation under the direction of the p40 promoter. The three capsid

subunits, VP1, VP2 and VP3 (MW: 87 kDa, 73 kDa, and 62 kDa, respectively), self-assemble to form the 60-mer capsid in a stoichiometric ratio of 1:1:10 (VP1:VP2:VP3)<sup>5-7</sup>. In addition, an alternative open reading frame of the *cap* gene encodes the assembly activating protein (AAP), which promotes virion assembly<sup>10</sup>. To establish latency, the AAV genome integrates into a genomic locus, *AAVS1*, as a provirus in human cells<sup>11</sup>. An explanation for this cellular event is because of the sequence similarity between *AAVS1* and the ITR and Rep activity.

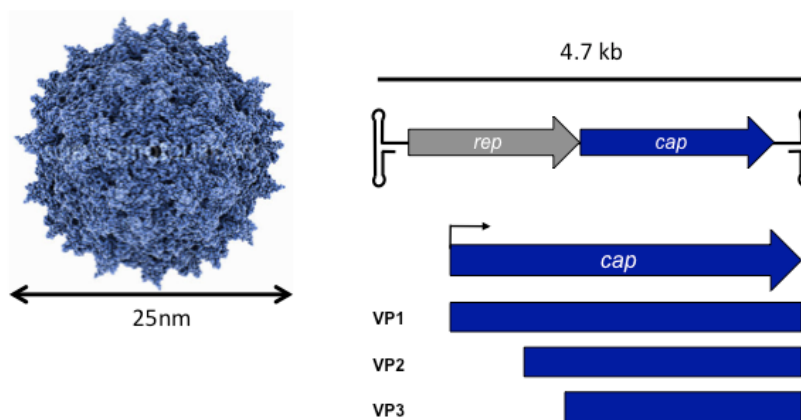


**Figure 1-2. AAV Structure and Genome.** The AAV genome is 25nm in diameter. The viral capsid proteins (VPs) assemble together in 60 subunits to form the capsid shell. Its viral genome is 4.7kb and is comprised of the *rep* and *cap* genes. The *cap* gene encodes for three structural proteins (VP1, VP2, VP3) that assemble together in a 1:1:10 stoichiometric ratio to form the AAV capsid<sup>8,9</sup>. Figure used with publisher's permission.

### *AAV Intracellular Trafficking*

AAVR is an essential AAV receptor for multiple serotypes and facilitates intracellular trafficking<sup>12</sup>. Upon receptor recognition, AAV is endocytosed into the host cell (**Figure 1-3**)<sup>5</sup>. Intact AAV particles enter the endosomal pathway to undergo a series of pH-dependent structural changes necessary

for viral trafficking. After endosomal escape, AAV enters the nucleus through the nuclear pore complex. Within the nucleus, AAV undergoes capsid uncoating and releases its single-stranded DNA genome.

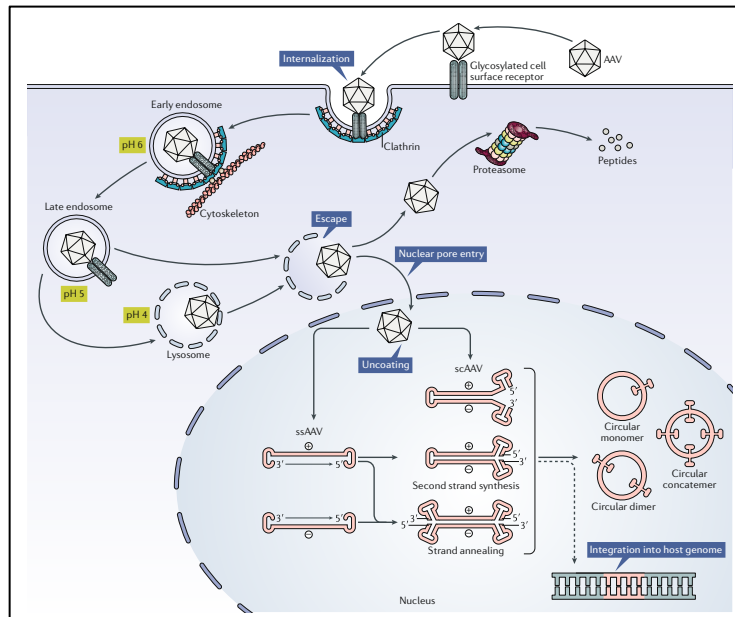


**Figure 1-3. AAV Cellular Trafficking.** AAV enters the cell via clathrin-mediated endocytosis. Following internalization, AAV enters the endosomal pathway where it undergoes a conformational change due to the acidic environment. Then, it enters the nucleus to uncoat its capsid and to release its genome for transgene expression <sup>13</sup> Figure used with publisher’s permission.

The released single-stranded AAV genome is converted to a double-stranded form. This conversion, known as second-strand synthesis, is required for transcription and a rate-limiting step for transduction. Second strand synthesis starts from the self-primed ITR at the 3'-end of the genome. Following second strand synthesis, the double-stranded genome of recombinant AAV (rAAV) circularizes via intra-molecular or inter-molecular genome recombination at the ITRs. The circularization process leads to rAAV

genome stabilization as episomal DNA that allows persistence of gene expression in nondividing cells.

To bypass the rate-limiting step of second-strand synthesis, self-complementary AAV (scAAV) vectors were designed to circumvent the ssDNA to dsDNA conversion<sup>14</sup>. A scAAV vector has an encapsidated genome that contains both plus and minus ssDNA structures that assemble to form a dsDNA molecule<sup>15</sup>. Typically, scAAV vectors display high levels of transgene expression in *in vitro* and *in vivo* models<sup>16</sup>. However, reduced transgene size (~2.5kb) compared to the single-stranded DNA (ssDNA) genome is a major limitation for AAV technology<sup>16</sup>.

#### *AAV Immune Response*

Epidemiological studies have shown that 40–80% of the human population has anti-AAV antibodies<sup>17</sup>. The AAV serotypes AAV1, AAV2, AAV3, AAV5, and AAV6 are endemic to humans, which implies that pre-existing AAV capsid immunity may be a constraint in successful transduction efficacy of AAV-based gene therapy technology<sup>18-21</sup>. To overcome this barrier for AAV gene therapy, understanding the adaptive response against the transgene and capsid will provide knowledge in addressing these issues.

#### *AAV Transgene Immune Response*

Clinical subjects do not express protein from genes that contain null mutations. Consequently, these patients lack self-tolerance against the gene product and represent the most challenging immune need for tolerance of foreign therapeutic transgenes. Upon cellular processing, antigen-presenting cells display transgene product fragments on their surface. This

process is a major barrier towards successful gene delivery. To address these issues, researchers have discovered that the development of transgene immune responses is dependent on the route of administration. Previously, AAV preclinical studies demonstrated that intramuscular injection may allow persistent transgene expression in nontolerant animal models. Based on these clinical successes, direct intramuscular injections for AAV gene transfer were used for a number of diseases: hemophilia B, lipoprotein lipase deficiency, cardiac failure, and muscular dystrophy. For these studies, transgene immune responses were not observed <sup>22</sup>. Conversely, for a Duchenne muscular dystrophy study for AAV gene therapy in children, transgene expression was hindered in all 6 subjects <sup>22</sup>. In addition, muscle biopsies indicated the presence of transgene-specific CD4<sup>+</sup> and CD8<sup>+</sup> T cells in 4 of 6 subjects <sup>22</sup>. For another study using intramuscular gene transfer to treat  $\alpha_1$ -antitrypsin deficiency, researchers found CD4<sup>+</sup> and CD8<sup>+</sup>T-cells associated with circulating levels of transgene product <sup>22</sup>. Since intramuscular delivery may lead to transgene immune responses, alternative targeting strategies have been developed. Key developments demonstrate that muscle targeting via an intravascular route may lead to lower transgene immunogenicity, thus higher transduction efficiency <sup>22</sup>.

#### *AAV Capsid Immune Response*

As a gene therapy vector, AAV was considered to have minimal immunogenicity. However, neutralizing antibodies (NAbs) were discovered worldwide in healthy subjects or in specific populations for gene therapy. Because of high pre-existing NAbs levels, at least 50% of patients were

excluded for gene therapy studies. In earlier AAV clinical trials for factor IX, a subset of patients had preexisting NABs, while others had an AAV capsid-specific CD8+ cytotoxic T cell response<sup>22</sup>. Ultimately, the CD8+ cytotoxic T cell response caused a decline in factor IX expression. For a subsequent clinical trial for hemophilia B using AAV8, patients were also excluded because of NABs against the capsid<sup>22</sup>. Additionally, capsid-specific T cell responses were detected. Increased aspartate and alanine aminotransferase blood levels determined these immune responses, while plasma factor IX levels decreased<sup>23</sup>. For muscle and immune-privileged regions, capsid T-cell responses were low resulting in no loss of therapeutic efficacy. Overall, the drawbacks of the human immune response to AAV capsid were mainly shown in the hemophilia B (factor IX deficiency) trials. Bioengineering of AAV vectors must be implemented to circumvent the AAV immune response and to improve safety and efficacy of AAV gene transfer in clinical settings.

### **\*AAV Capsid Bioengineering**

Viruses can be engineered to exhibit altered functionalities through the insertion of bioactive peptides and proteins into the capsid. The peptides and proteins can be completely foreign to viruses in general. This genetic modification strategy necessitates the identification of a capsid site that fulfills the following criteria: 1) tolerance to the insertion, resulting in maintenance of important virus properties, such as capsid assembly, genome packaging, and infectivity; 2) maintenance of desired functional

properties of the inserted domain; and 3) if appropriate, overwriting of any<sup>8</sup> undesired innate virus properties (e.g. natural tropism). Such ideal capsid insertion sites can be identified through systematic mutagenesis efforts and structural studies. Going forward, molecular modeling strategies may be a promising approach to identifying optimal insertion sites *in silico*. For example, the AAV2 capsid residue 453 was identified as an alternative site for inserting a targeting peptide, instead of the commonly used residue 587, due to its prominence on the three-fold axis of symmetry as visualized through modeling. Below, we discuss ongoing efforts to insert peptides/proteins into rationally chosen capsid sites as well as into random locations throughout the capsid in an attempt to identify optimal insertion sites<sup>24</sup>.

#### *Rational insertion of defined peptide/protein*

For adenoviral vectors, the fiber knob region continues to be the insertion site of choice, for both small and large peptides. The HI loop is highly variable across serotypes and has been shown to tolerate insertions, and by inserting the A20FMDV2 peptide into this region, Coughlan et al. were able to retarget Ad5 to  $\alpha v\beta 6$  integrin, an epithelial integrin significantly upregulated in many carcinomas. After systemic *in vivo* delivery, the mutated virus demonstrated increased transduction of tumor cells and decreased off-target transduction of the liver. The NGR peptide has also

---

\* For this section, this was published in Wiley Interdiscip Rev Nanomed Nanobiotechnol. **2014**

been used to retarget Ad5 from CAR to aminopeptidase N, expressed by endothelial cells and upregulated in some cancers. However, both retargeted vectors continue to demonstrate high liver uptake and other off-target biodistribution, indicating that small peptides may not be sufficient for complete retargeting. Beyond retargeting efforts, small peptide insertions have been used to reduce the immune response against adenovirus. Ad vectors that displayed the decay-accelerating factor (DAF), a human complement inhibitor, through fusion to the C terminus of the pIX capsid protein exhibited dramatically reduced immune responses in mice. The adenovirus HI loop is also amenable to larger peptide insertions, such as the insertion of two different Affibody molecules into the same fiber knob, leading to dual binding specificity. Antibodies have also been inserted into the adenovirus capsid; however, mutants with single-chain antibody fragment insertions are unable to retarget due to improper folding of the antibody. However, by fusing the single-domain antibody AFAI to the pIX capsid protein, Poulin et al. were able to successfully incorporate the antibody into adenovirus and retarget the vector to cells expressing CD66c, a marker upregulated in lung carcinomas. For AAV vectors, the N-terminus of the VP2 capsid subunit has been identified as a site amenable for peptide/protein insertions. Designed ankyrin repeat proteins (DARPin) have been incorporated into this location in order to retarget AAV2 to cells expressing HER2/neu<sup>25</sup>. Promisingly, the AAV-DARPin vectors demonstrated tumor-targeting capabilities with decreased transgene expression in off-target organs, such as the liver. Lentiviruses have also been modified with

proteins not endogenous to viruses. For example, antibodies were modified to become membrane-bound and incorporated into the lentiviral envelope with pH-dependent fusogenic proteins, creating a viral vector that targets CD20-expressing cells both *in vitro* and *in vivo* <sup>24</sup>.

#### *Rational insertion of random peptide*

Over the last several decades, many targeting peptides have been identified through phage display– viral libraries that display some number of random amino acid residues in a specific site on a coat protein. It can be difficult, however, to predict if the peptide (identified in the context of the bacteriophage) will function similarly once placed in the framework of a different virus capsid. Additionally, peptides selected from phage display may mediate cell binding, but may not necessarily support downstream steps of the gene delivery process. To overcome these limitations, viral gene delivery vectors, rather than bacteriophage, have been used to create peptide display libraries that can be selected/screened *in vitro* or *in vivo* to identify new variants with desired properties. A number of viruses have been subjected to random peptide display and directed evolution. Bupp et al. generated a random peptide display library on the feline leukemia virus subgroup A and demonstrated that applying appropriate selection pressures on this library can result in identification of fully functional viral vectors with altered cell specificity. For the adenovirus platform, Miura et al. developed an improved method for high efficiency peptide display library generation. This method uses a fiberless adenovirus and relies on intracellular CRE-lox-mediated recombination between a library of fiber-encoding shuttle plasmids

and the fiberless adenovirus genome. The library was used to identify a virus variant with selective infectivity for mesothelin-positive cells both *in vitro* and *in vivo*. Nishimoto et al. used *in vivo* selection to obtain peritoneal tumor-targeting Ad vectors from random peptide display libraries. The peptide display approach was also applied to AAV serotype 2 (AAV2) by inserting a randomized seven-residue peptide into the receptor binding domain of the virus. Upon selection, an AAV mutant was isolated with preferential transduction of coronary artery endothelial cells, which are weakly transduced by wt capsid AAV2 vectors. *In vivo* selection of an AAV2 peptide display library also led to identification of heart-targeting vectors in mice. Overall, peptide display has been carried out successfully in the context of several different viruses. Although conceptually easy to understand, directed evolution approaches to generating improved viral vectors have many challenges in practice. Producing naïve viral libraries (pre-selection) free of wt vectors can be difficult; therefore, selection may be overwhelmed if performed on cells susceptible to the wt vector. Additionally, native tropism may not be ablated by peptide display, leading to the expansion of, rather than a replacement of, tropism<sup>24</sup>.

#### *Random insertion of defined peptide/protein*

In certain instances, the challenge may not be identification of the targeting peptide but rather identification of the optimal capsid insertion site. In this case, the defined peptide/protein can be inserted randomly throughout the capsid, and application of the appropriate selection pressure will help isolate the desired mutants. One way to carry out random insertion

is through the use of DNase I. The nuclease digestion is optimized to create single breaks in double-stranded DNA at random locations. The peptide/protein is then ligated into the cut site, yielding a library of viral genes with peptides/proteins inserted randomly throughout. The approach was first applied to viral vectors in the context of AAV serotype 5 (AAV5) to identify capsid regions tolerant to deletions and duplications. This method was taken a step further to generate a platform library, named RaPID (random peptide insertion by DNase), which could be used to insert desired peptides/proteins randomly throughout the AAV2 capsid gene in a facile manner. Selection of the virus library can then identify capsid insertion sites that fulfill the design criteria set forth in the beginning of this section. Using this library, an AAV2 capsid insertion site was identified that is tolerant to mCherry insertion. Notably, the insertion site was in the VP3 region of the *cap* gene – part of the capsid previously thought to be intolerant to the insertion of relatively large proteins. The isolated mutant was not only fluorescent but also exhibited similar infectivity to wt capsid. Alternatively, transposase-mediated random insertion can be used to insert peptides/proteins into viral capsids. For example, this approach was used to insert hexahistidine tags into the AAV2 capsid, yielding viral mutants able to be captured on nickel affinity columns. A commercially available kit is available for transposase-mediated random insertion, rendering the mutagenesis process to be more streamlined. The DNase-based method, although lacking a commercial kit to our knowledge, introduces additional crossover diversity in the form of deletions and duplications. In summary,

viral vectors can be designed to exhibit properties foreign to natural viruses by genetically incorporating bioactive peptides/proteins into the capsid. Known peptides/proteins can be inserted into the capsid at rationally chosen sites, or the optimal insertion site can be identified through combinatorial random domain insertion approaches. Alternatively, random peptides can be inserted into rationally chosen capsid locations in order to identify a bioactive peptide motif that would bestow upon the virus the desired phenotype <sup>24</sup>.

#### *Tweaking viruses through point mutations*

In certain instances, introducing point mutations to a pre-existing virus capsid, either nature-derived or human-engineered, may be all that is needed to obtain the optimal vector. The point mutations can be scattered throughout a gene, or clustered in a rationally chosen capsid domain <sup>24</sup>.

#### Random point mutations

Error-prone polymerase chain reaction (EP-PCR) has been used to create libraries containing AAV capsid genes with point mutations throughout. Application of appropriate selection pressures resulted in vectors capable of evading neutralizing antibodies. Using EP-PCR on AAV, Asuri et al. generated a virus variant that was able to more efficiently deliver a genetic payload to human stem cells. They further enhanced this vector by coupling it with the delivery of a zinc-finger nuclease to promote homologous recombination of the delivered transgene through induced double-strand breaks, thus enabling gene targeting. EP-PCR coupled with *in vivo* selection also led to the generation of a novel AAV vector capable of transducing outer

retinal cells after injection into the vitreous humor. The *in vivo* selection was key in isolating vectors that can migrate through complex extracellular environments to reach the desired cell population. Lastly, rather than creating mutations throughout the capsid, Pulicherla et al. took advantage of structure-function knowledge and generated an AAV library with random mutations focused in the VP3 GH loop, a region that is highly variable between AAV serotypes and previously identified to impact tropism in AAV serotype 9. Through directed evolution, they were able to identify an AAV9 variant with decreased tropism for the liver, but retained wt transduction levels in cardiac and skeletal muscle. In summary, modification of viral properties may only require a small number of point mutations, identified in a completely random fashion (i.e. mutations scattered throughout capsid), or in a pseudo-rational manner (i.e. mutations localized to rationally chosen capsid region). These mutations can be layered on top of naturally occurring capsids or those engineered previously through other means <sup>24</sup>.

#### *Rational point mutations*

In AAV intracellular trafficking, the ubiquitin–proteasome pathway is a key factor and the epidermal growth factor receptor protein tyrosine kinase (EGFR-PTK) signaling modulates the pathway <sup>26</sup>. Zhong et al. discovered that EGFR-PTK signaling allows efficient AAV transduction and second strand synthesis due to increased viral trafficking from the cytoplasm to the nucleus. Also, the researchers demonstrated *in vitro* that EGFR-PTK signaling is responsible for tyrosine phosphorylation on the AAV capsid <sup>27</sup>. Based these results, the authors suggested that tyrosine phosphorylation is

responsible for ubiquitin signaling and proteasomal degradation in the cytoplasm before virion nuclear entry. Following these findings, continued investigation with site directed mutagenesis of surface exposed tyrosines (tyrosine (Y) to phenylalanine (F)) on the AAV capsid (Y252, Y272, Y444, Y500, Y700, Y704, and Y730) exhibited increased transduction efficiency in both *in vitro* and *in vivo* models. Additionally, serines (S) and threonines (T) are potential sites for both phosphorylation and ubiquitination events on the AAV capsids. Sen et al. conducted alanine screen mutagenesis of S/T residues (AAV2-S489A, S662A, T251A, K544R, AAV5-S652A, AAV1-S669A, AAV8-K137R, S671A), which resulted in AAV vectors exhibiting higher transgene expression and reduced NAb production <sup>26</sup>. To summarize, rational point mutations on AAV capsids is a promising approach to gain knowledge for AAV transduction optimization.

## **Thesis Overview**

This thesis presents an aspiration to uncover design rules for improving AAV targeting, transduction efficiency, and immune-avoidance. Chapter 2 illustrates the importance of peptide lock amino-acid properties that dictate the function of protease-activatable AAV vectors that are responsive to enzymatic biomarkers. Chapter 3 describes an engineered immuno-AAV vector that evades phagocytic cells. Chapter 4 explores critical serine residues essential for viral transduction. In summary, this work shares the research efforts on the design, construction, and characterization of AAV mutants to improve gene delivery efficacy and specificity.

## REFERENCES

- (1) Dunbar, C. E.; High, K. A.; Joung, J. K.; Kohn, D. B.; Ozawa, K.; Sadelain, M. Gene therapy comes of age. *Science* **2018**, *359*, eaan4672.
- (2) Jenks, S. Gene Therapy Death — "Everyone Has to Share in the Guilt". *JNCI: Journal of the National Cancer Institute* **2000**, *92*, 98-100.
- (3) Nienhuis, A. W.; Dunbar, C. E.; Sorrentino, B. P. Genotoxicity of retroviral integration in hematopoietic cells. *Mol Ther* **2006**, *13*, 1031-1049.
- (4) Cavazzana-Calvo, M., Hacein-Bey, S., de Saint Basile, G., Gross, F., Yvon, E., Nusbaum, P., Selz, F., Hue, C., Certain, S., Casanova, J.L. and Bouso, P., . Gene Therapy of human severe combined immunodeficiency (SCID)-X1 disease. *Science* **2000**, *288*, 669-672.
- (5) Wang, D.; Tai, P. W. L.; Gao, G. Adeno-associated virus vector as a platform for gene therapy delivery. *Nat Rev Drug Discov* **2019**, *1*.
- (6) Padron, E.; Bowman, V.; Kaludov, N.; Govindasamy, L.; Levy, H.; Nick, P.; McKenna, R.; Muzyczka, N.; Chiorini, J. A.; Baker, T. S.; Agbandje-McKenna, M. Structure of adeno-associated virus type 4. *J Virol* **2005**, *79*, 5047-5058.
- (7) Xie, Q.; Bu, W.; Bhatia, S.; Hare, J.; Somasundaram, T.; Azzi, A.; Chapman, M. S. The atomic structure of adeno-associated virus (AAV-2), a vector for human gene therapy. *Proc Natl Acad Sci U S A* **2002**, *99*, 10405-10410.
- (8) O'Donnell, J.; Taylor, K. A.; Chapman, M. S. Adeno-associated virus-2 and its primary cellular receptor--Cryo-EM structure of a heparin complex. *Virology* **2009**, *385*, 434-443.

(9) Schmidt, M.; Govindasamy, L.; Afione, S.; Kaludov, N.; Agbandje-McKenna, M.; Chiorini, J. A. Molecular characterization of the heparin-dependent transduction domain on the capsid of a novel adeno-associated virus isolate, AAV(VR-942). *J Virol* **2008**, *82*, 8911-8916.

(10) Florian Sonntag, K. S., and Jurgen A. Kleinschmidt. A viral assembly factor promotes AAV2 capsid formation in the nucleolus. *PNAS* **2010**, *107*, 10220-10225.

(11) Kotin, R. M., Marcello Siniscalco, R. Jude Samulski, X. D. Zhu, Lynne Hunter, Catherine A. Laughlin, Susan McLaughlin, Nicholas Muzyczka, Marino Rocchi, and Kenneth I. Berns. . Site-specific integration by adeno-associated virus. *Proceedings of the National Academy of Sciences* **1990**, *87*, 2211-2215.

(12) Pillay, S.; Meyer, N. L.; Puschnik, A. S.; Davulcu, O.; Diep, J.; Ishikawa, Y.; Jae, L. T.; Wosen, J. E.; Nagamine, C. M.; Chapman, M. S.; Carette, J. E. An essential receptor for adeno-associated virus infection. *Nature* **2016**, *530*, 108-112.

(13) Wang, D.; Tai, P. W. L.; Gao, G. Adeno-associated virus vector as a platform for gene therapy delivery. *Nat Rev Drug Discov* **2019**.

(14) Ferrari, F. K., Samulski, T., Shenk, T. and Samulski, R.J. Second-strand synthesis is a rate-limiting step for efficient transduction by recombinant adeno-associated virus vectors. *Journal of virology* **1996**, *70*, 3227-3234.

(15) McCarty, D. M., Fu, H., Monahan, P.E., Toulson, C.E., Naik, P. and Samulski, R.J. Adeno-associated virus terminal repeat (TR) mutant

generates self-complementary vectors to overcome the rate-limiting step to transduction in vivo. *Gene therapy* **2003**, *10*, 2112.

(16) McCarty, D. M. Self-complementary AAV vectors; advances and applications. *Mol Ther* **2008**, *16*, 1648-1656.

(17) Calcedo, R.; Morizono, H.; Wang, L.; McCarter, R.; He, J.; Jones, D.; Batshaw, M. L.; Wilson, J. M. Adeno-associated virus antibody profiles in newborns, children, and adolescents. *Clin Vaccine Immunol* **2011**, *18*, 1586-1588.

(18) Sylvie Boutin, V. M., Philippe Veron, Christian Leborgne, Olivier Benveniste, Marie Françoise Montus, and Carole Masurier. Prevalence of Serum IgG and Neutralizing Factors Against Adeno-Associated Virus (AAV) Types 1, 2, 5, 6, 8, and 9 in the Healthy Population: Implications for Gene Therapy Using AAV Vectors. *HUMAN GENE THERAPY* **2010**, *21*, 704-712.

(19) Chen, C. L.; Jensen, R. L.; Schnepf, B. C.; Connell, M. J.; Shell, R.; Sferra, T. J.; Bartlett, J. S.; Clark, K. R.; Johnson, P. R. Molecular characterization of adeno-associated viruses infecting children. *J Virol* **2005**, *79*, 14781-14792.

(20) Calcedo, R.; Vandenberghe, L. H.; Gao, G.; Lin, J.; Wilson, J. M. Worldwide epidemiology of neutralizing antibodies to adeno-associated viruses. *J Infect Dis* **2009**, *199*, 381-390.

(21) Boutin, S., Monteilhet, V., Veron, P., Leborgne, C., Benveniste, O., Montus, M.F. and Masurier, C. Prevalence of serum IgG and neutralizing factors against adeno-associated virus (AAV) types 1, 2, 5, 6, 8, and 9 in the

healthy population: implications for gene therapy using AAV vectors. *Human gene therapy* **2010**, *21*, 704-712.

(22) Mingozi, F.; High, K. A. Immune responses to AAV vectors: overcoming barriers to successful gene therapy. *Blood* **2013**, *122*, 23-36.

(23) Nathwani, A. C., Tuddenham, E.G., Rangarajan, S., Rosales, C., McIntosh, J., Linch, D.C., Chowdary, P., Riddell, A., Pie, A.J., Harrington, C. and O'beirne, J. Adenovirus-associated virus vector-mediated gene transfer in hemophilia B. *New England Journal of Medicine* **2011**, *365*, 2357-2365.

(24) Caitlin M. Guenther, B. E. K., Michael T. Lam, Tawana M. Robinson, Julia Zhao, and Junghae Suh. Synthetic Virology: Engineering Viruses for Gene Delivery. *Wiley Interdisciplinary Reviews: Nanomedicine and Nanobiotechnology* **2014**, *6*, 548-558.

(25) Munch, R. C.; Janicki, H.; Volker, I.; Rasbach, A.; Hallek, M.; Buning, H.; Buchholz, C. J. Displaying high-affinity ligands on adeno-associated viral vectors enables tumor cell-specific and safe gene transfer. *Mol Ther* **2013**, *21*, 109-118.

(26) Buning, H.; Srivastava, A. Capsid Modifications for Targeting and Improving the Efficacy of AAV Vectors. *Mol Ther Methods Clin Dev* **2019**, *12*, 248-265.

(27) Zhong, L.; Zhao, W.; Wu, J.; Li, B.; Zolotukhin, S.; Govindasamy, L.; Agbandje-McKenna, M.; Srivastava, A. A Dual Role of EGFR Protein Tyrosine Kinase Signaling in Ubiquitination of AAV2 Capsids and Viral Second-strand DNA Synthesis. *Molecular Therapy* **2007**, *15*, 1323-1330.

# **Chapter 2: Role of Tetra Amino Acid Motif**

## **Properties on the Function of Protease-Activatable**

### **Viral Vectors**

#### **INTRODUCTION**

Extracellular proteases, such as matrix metalloproteinases (MMPs), are elevated at sites of disease in various pathologies, such as cancer<sup>1</sup> and cardiovascular diseases.<sup>2</sup> Increased MMP activity has been implicated in disease progression and, thus, has been used as a biomarker to target therapeutics to affected tissues.<sup>2-8</sup> For example, Ge et al. developed a polyethylenimine-gelatin gene delivery vector that upon MMP cleavage becomes activated to interact with the target cell membrane.<sup>9</sup> More recently, Gjetting et al. synthesized lipo-nanoparticles with a lipid moiety that is susceptible to protease cleavage for delivery to diseased sites.<sup>10</sup> Several viral vectors, including retrovirus and measles virus,<sup>11,12</sup> have also been engineered to be protease-responsive. Thus, activation by an intrinsic biomolecular stimulus,<sup>13</sup> such as an extracellular protease, is proving to be a promising approach for targeted therapy. Previously, we constructed a protease-activatable virus (Provector) based on adeno-associated virus serotype 2 (AAV2) that delivers transgenes upon activation by MMPs.<sup>17</sup> AAV is a promising delivery vector for gene therapy of various human diseases,<sup>15</sup> including cancer.<sup>16</sup> Our design strategy involves the insertion of a "peptide

lock” into the heparan sulfate proteoglycan (HSPG) binding region in the AAV2 capsid.<sup>17</sup> The prototype peptide lock consists of a tetra amino acid motif (4AA motif), comprising four negatively charged aspartic acids, flanked by MMP cleavage consensus sequences (**Figure 2-1**). With the peptide locks in place, the provectors are unable to transduce cells. Then, in the presence of target MMPs, the peptide locks are cleaved off the capsid, allowing the viruses to regain their ability to bind HSPG and deliver transgenes.

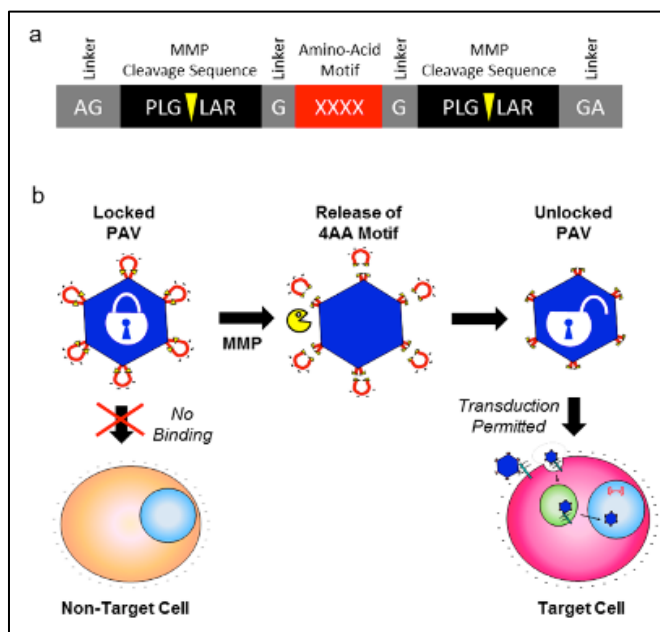


**Figure 2-1. Protease-activatable virus (provector) design and concept.** (a) Peptide lock consists of the tetra amino acid (4AA) motif flanked by MMP cleavage consensus sequences. Scissile bonds are indicated by yellow arrows. Glycine linkers separate the MMP consensus sequences and the 4AA motif. (b) Peptide locks inserted into the AAV capsid prevent virus binding to cellular receptors. In the presence of MMPs, the MMP consensus sequences are cleaved, releasing the peptide locks from the capsid and restoring viral transduction.

\*For Chapter 2, this was published in ACS Biomaterials Science and Engineering. **2016**, 2, 2026–2033. doi:10.1021/acsbomaterials.6b00439.

We have demonstrated that our vector works well in exhibiting protease-switchable transduction behavior.<sup>17,18</sup> However, a question that remained was whether the aspartic acid residues of the 4AA motif were optimal for peptide lock operation or if other amino acids may be used as the 4AA motif. The tetra-aspartic acids were initially chosen because we hypothesized that the negatively charged amino acids inserted into the receptor binding domain of AAV2 would electrostatically repel the binding of negatively charged HSPG by the virus capsid. Effective HSPG binding by the patch of positively charged amino acid residues on the AAV2 capsid is required for successful cellular transduction.<sup>19</sup> To address this question, I synthesized and characterized provector mutants with different 4AA motifs to study the effect of motif chemical properties on provector function. Our results suggest tetra-aspartic acid and tetra- glutamic acid motifs yield the best provector properties to date.

## **RESULTS**

### **Production of Viruses with Peptide Lock Variants**

I synthesized a panel of provector variants to test the effects of 4AA motif properties on virus production and performance. Quantitative polymerase chain reaction (qPCR) was used to quantify the titers of the provector variants produced (**Figure 2-2**).

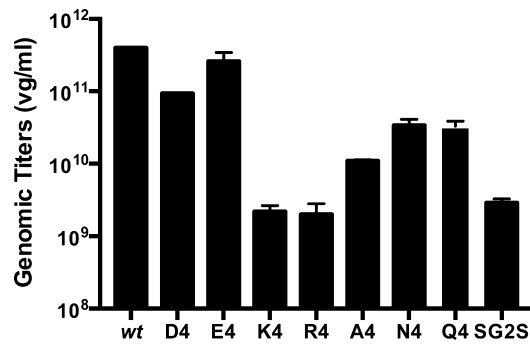


**Figure 2-2. Titers of Provector candidates with different tetra amino acid (4AA) motifs.** D4, tetra aspartic acid. E4, tetra glutamic acid. K4, tetra lysine. R4, tetra arginine. A4, tetra alanine. N4, tetra asparagine. Q4, tetra glutamine. SG2S, serine-glycine-glycine-serine. Virus titers were quantified with qPCR. Standard error of the mean (SEM) of two independent virus preparations are shown. All mutant titers are statistically different compared to wt ( $p < 0.001$ , student t test), with the exception of Provector-E4.

The viruses with negatively charged 4AA motifs, provector-D4 and provector-E4, yield titers that are within 1-log of wild-type (wt), indicating these motifs do not adversely impact virus capsid assembly and genome packaging. Provector-A4, -N4, and -Q4, are within 1<sup>2</sup> log of wt. The positively charged 4AA motif mutants, Provector-K4, -R4, and the polar uncharged -SG2S display the most dramatic decreases in titers that are 2-log fold lower than wt. Therefore, the AAV capsid appears to be most tolerant to peptide locks with negatively charged 4AA motifs and poorly tolerates positively charged 4AA motifs. Western blot was performed to detect viral capsid proteins (VPs) and qualitatively assess peptide lock incorporation into the capsid (**Figure 2-3**). Because the iodixanol density gradient separation process collects assembled capsids, and these separated virus samples are the ones run on the Western blot, the bands in (**Figure 2-3**) capture the VP subunit profiles in the assembled capsid.

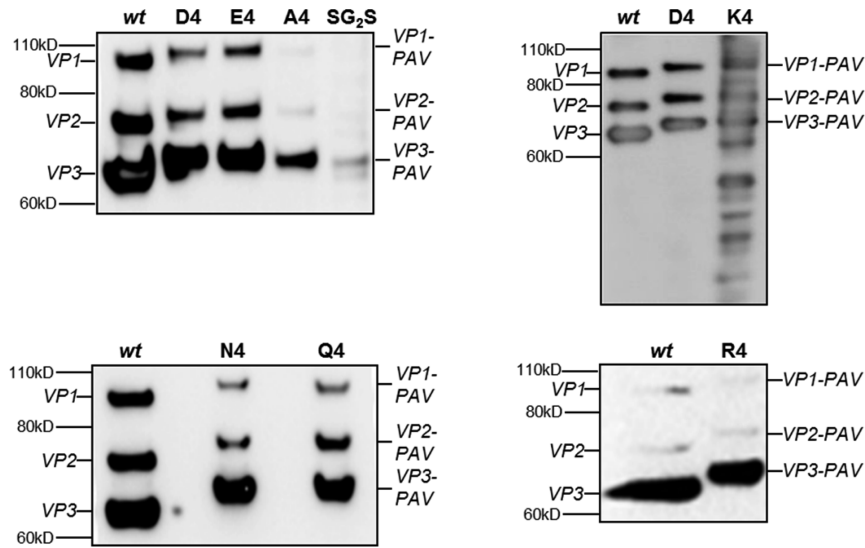


**Figure 2-3. Detection of viral capsid proteins (VPs) and peptide lock incorporation of provector candidates via Western blot.** Same volume of iodixanol- separated virus was loaded per well, except for the R4 blot in which the same number of viral genomes were loaded for wt and R4. Capsid subunits were probed with the B1 antibody, which detects a c-terminal epitope shared among all three VPs. VP1, VP2, and VP3 indicate wt capsid subunits. VP1-Provectpr, VP2-Provector, and VP3-Provector indicate capsid subunits with peptide lock insertions. Molecular weight ladder locations are indicated on the left side of blots. Most virus variants display only three VP bands similarly to wt capsid. Provector-K4 displays an irregular pattern of multiple bands beyond the expected three VP bands.

Most provector variants display VP expression patterns similar to wt, although with a noticeable MW shift due to peptide lock insertion. These results indicate the peptide locks are successfully inserted into the VP subunits and the subunits are able to assemble into the capsid. The VP band intensities of the provector-A4 and provector-SG2S viruses are lighter compared to other mutants because they had lower genomic titers. Interestingly, the provector-K4 variant displays an irregular pattern with multiple VP fragments on the Western blot, which may suggest increased susceptibility of provector-K4 to trypsin and potentially other proteases

during virus production.<sup>21</sup> Considering the qPCR and Western blot data together, the provector mutants demonstrate successful peptide lock insertion, capsid assembly, and genome packaging, albeit at lower levels compared to *wt* for most of the mutants.

### **Capsid Stability of Viruses with Peptide Lock Variants**

Next, I tested the stability of the formed capsids using a nuclease protection assay. A stable, well-formed capsid should effectively protect its encapsidated genome from degradation by nucleases. Provector mutants were treated with benzonase and the level of genome protection was quantified with qPCR (**Figure 2-4**). As expected, the *wt* control displays full genome protection, while the negative control (naked plasmid DNA) exhibits complete degradation. Provectors -R4, -A4, -N4, -Q4, and -SG2S exhibit *wt*-like abilities to protect their genomes. Thus, although these variants are produced at lower titers than *wt*, the assembled capsids are stable. Provectors -D4 and -E4, produced at *wt*-like titers, show protection levels slightly less than *wt* but the differences are not statistically significant. Provector -K4 has the lowest level of genome protection, which could potentially be due to protease susceptibility during capsid assembly, as suggested by Western blotting. The provector-K4 virus appears to be the most defective virus thus far, with a low production titer, an irregular VP band pattern, and lowest capsid stability.

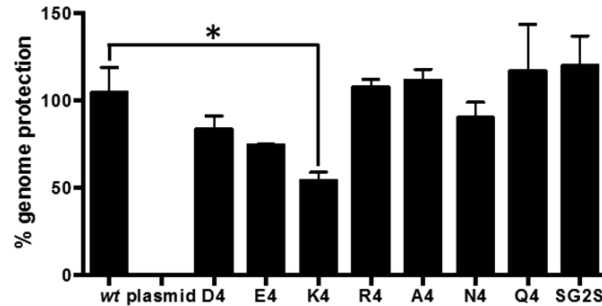


**Figure 2-4. Capsid stabilities of Provector candidates as assessed by their abilities to protect their genomes from nuclease digestion.** Provector candidates were incubated with benzonase nuclease to measure capsid stability. % genome protection was quantified with qPCR. Naked plasmid DNA is used as a control to ensure nuclease activity. Error bars represent SEM of two independent experiments performed in duplicate. Asterisk indicates  $p < 0.05$  by student t test.

### Impact of Peptide Lock Variants on Heparin Binding

I conducted a heparin affinity assay to test if 4AA motif properties play a role in locking the virus. A successful peptide lock design should ablate heparin binding by the virus in absence of proteases. Our wt positive control elutes from the heparin resin at 500 mM NaCl and higher (**Figure 2-5**) as expected from previous reports.<sup>17,20</sup> AAV serotype 4 (AAV4) serves as the negative control for this assay because it binds sialic acid instead of heparin.<sup>22</sup> As expected, the majority of AAV4 do not bind the heparin coated beads. Most of the provector mutants display low heparin binding, with the exception of the three polar uncharged motifs (SG2S, N4, and Q4) that appear to retain intermediate heparin binding ability. Overall, this data demonstrates negatively charged, positively charged, and hydrophobic 4AA motifs are successfully able to disrupt heparin binding by the vir

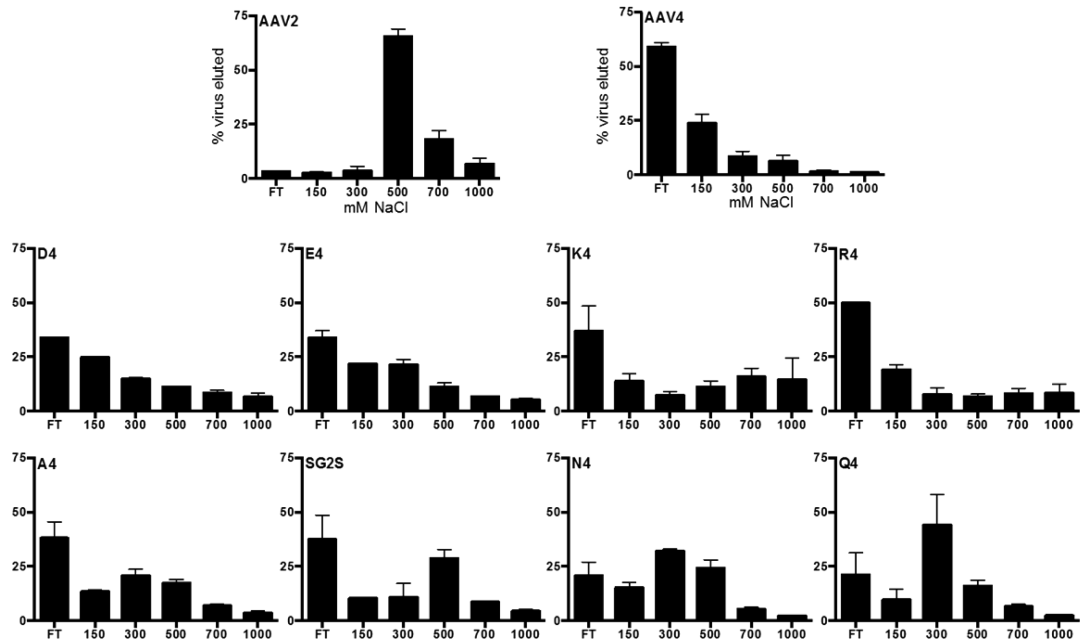


**Figure 2-5. Ability of various 4AA motifs to disrupt virus-heparin binding.** Viruses were eluted from heparin agarose beads by incubating with increasing NaCl concentration buffers. qPCR was used to measure virus amounts in the elutions. AAV serotype 2 (AAV2) binds to heparin and elutes off the heparin beads at 500-700 mM NaCl. AAV serotype 4 (AAV4) does not bind to heparin. Error bars represent SEM of two independent experiments.

### Ability of Peptide Lock Variants to Block Cellular Transduction

I performed a transduction assay to investigate whether various peptide locks are able to prevent cellular transduction by the viruses in the absence of proteases, as desired. In comparison to wt, all of the provector mutants demonstrate significantly lower gene delivery

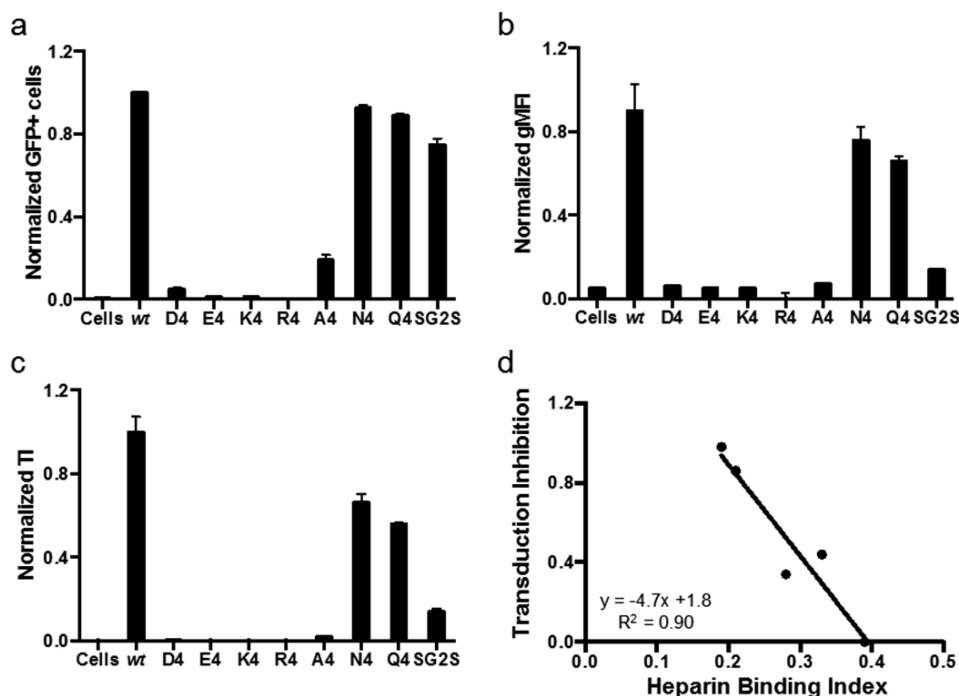


**Figure 2-6. Transduction assay to test if the various 4AA motifs are able to inhibit cellular transduction by provector candidates in the absence of proteases.** Viral genomes at a multiplicity of infection (MOI) of 500 were added to HEK293T cells. (a, b) %GFP+ cells and geometric mean fluorescence intensity (gMFI) were quantified with flow cytometry and normalized to wt values. (c) Transduction index (TI) is %GFP+ cells multiplied by gMFI and is a linear indicator of viral transduction efficiency.<sup>17</sup> Error bars represent SEM of two independent experiments conducted in duplicate. (d) Transduction inhibition as a function of heparin binding index. Lower the heparin binding index (i.e., less effective heparin binding ability), the better the inhibition of transduction in the absence of proteases. Data points for A4, SG2S, Q4, N4, and wt are plotted. The regression line is shown, with an R2 value of 0.90.

efficiencies (**Figure 2-6a,b,c**). The D4, E4, K4, R4, and A4 peptide locks are able to decrease the transduction index (TI) at least 6-fold compared to wt. N4, Q4, and SG2S are the least effective in blocking cellular transduction. N4 and Q4 decrease transduction 2-fold, while SG2S performs slightly better, yielding a 4- fold decrease. In summary, all inserted 4AA motifs with the exception of the polar uncharged motifs (N4, Q4, SG2S) appear to lock the

virus effectively regardless of chemical properties.

Considering the data gathered thus far, it appears that successful transduction inhibition by the peptide lock is correlated to the peptide lock's ability to prevent heparin binding. To develop a rough design "rule-of-thumb" that may help us screen through different future provector candidates, I calculated a heparin binding index for each candidate based on the results of the heparin affinity assay

heparin binding index

= (0.4) × (fraction eluted<sub>300 mM NaCl</sub>)

+ (0.6) × (fraction eluted<sub>500 mM NaCl</sub>)

The fraction of viruses eluting in the 500 mM NaCl fraction receive a greater weight of 0.6, compared to 0.4 for the 300 mM NaCl fraction, because these viruses have more wt AAV2-like heparin binding ability. Thus, a larger heparin binding index value indicates the virus retains more wt AAV2-like heparin binding ability. AAV2 and AAV4 have heparin binding indices of 0.39 and 0.06, respectively. Plotting the heparin binding index versus fraction transduction inhibition of the provector candidates (only those with less than complete inhibition) reveals a linear trend with an R<sup>2</sup> value of 0.9 (**Figure 2-6d**). The provector candidates with complete transduction inhibition (D4, E4, K4, and R4) all display heparin binding indices of less than 0.2. Peptide locks that yield low heparin binding index values (i.e., effective inhibition of heparin binding) are able to achieve greater transduction inhibition. Thus,

based on the results of the heparin binding assay, if a provector candidate displays a heparin binding index of less than 0.2, I can expect it to have successful complete transduction inhibition in the absence of proteases. Moving forward, the K4, R4, A4, N4, Q4, and SG2S variants were not analyzed further because of their suboptimal production titers (all six variants), an irregular VP band pattern and unstable capsid (K4), and incomplete locking of the capsid (N4, Q4, and SG2S).

### **Ability of Peptide Locks to Be Cleaved by Extracellular Proteases**

To determine whether the provector-E4 variant is susceptible to proteases and also regains the ability to transduce cells after protease detection, the virus was treated with matrix metalloproteinase 7 (MMP7) and assayed for capsid proteolysis and cellular transduction ability. Provector-D4 served as the positive control in these studies since we have previously shown this variant is proteolyzed by MMP7 and displays MMP-responsive transduction behavior.<sup>17</sup> A silver stain was performed to assess provector-E4 susceptibility to MMP7 (**Figure 2-7**). As expected, the wt negative control shows no protease susceptibility. In contrast, the provector-D4 positive control displays proteolytic susceptibility to MMP7, and not the sham condition.

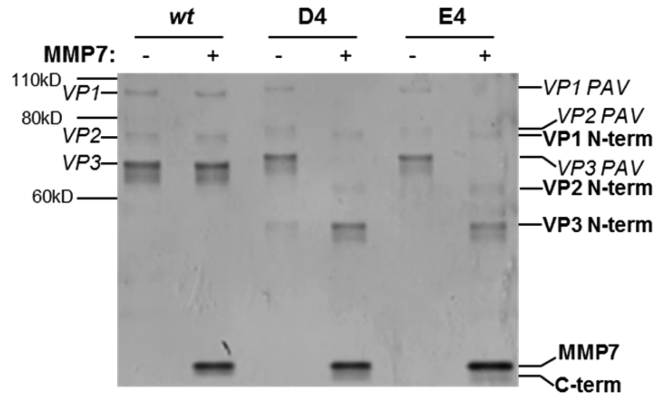


**Figure 2-7. Detection of proteolyzed VP fragments of Provector-D4 and Provector-E4 in the presence of MMP7.** Viruses were incubated in sham or MMP7 conditions, denatured, and then run on a 4"12% bis-tris gel. The gel was subsequently processed with the silver stain to visualize VP bands, either intact or proteolyzed. The band corresponding to the added MMP7 enzyme can be observed at the bottom of the image.

Provector-E4 demonstrates MMP susceptibility similar to provector-D4. This data indicates the negatively charged 4AA motifs, E4 and D4, are proteolyzed similarly by MMP7. Finally, I transduced HEK293T cells with viruses, with and without MMP treatment. In the presence of MMP7, provector-D4 and provector-E4 display increased gene delivery efficiencies compared to the sham condition (**Figure 2-8**). The provectors are less efficient compared to wt, which has been previously observed. Both of the tested provectors exhibit 2-fold lower TI values in the unlocked state (i.e., MMP treatment condition) compared to wt. These findings indicate provector-D4 and provector-E4 are able to regain transduction abilities in the presence of MMP7, albeit at a lower-than-wt efficiency.

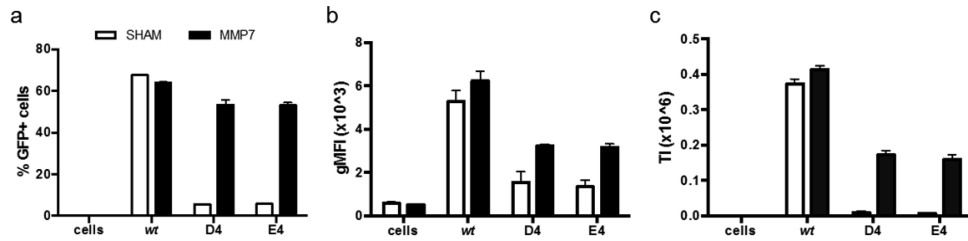


**Figure 2-8. Recovery of cellular transduction ability of Provector-D4 and Provector-E4 in the presence of MMP7.** Viral genomes at a multiplicity of infection (MOI) of 500 were added to HEK293T cells. %GFP+ cells and geometric mean fluorescence (gMFI) were quantified with flow cytometry. Error bars represent SEM of two independent experiments conducted in duplicate.

Taken together, these data demonstrate the negatively charged 4AA motifs, D4 and E4, are the best options among our panel of variants. On the basis of viral production titers, capsid assembly, receptor binding, and protease-activatable transduction abilities, the D4 and E4 variants appear to be functionally interchangeable.

## DISCUSSION

Prior work by others have demonstrated the AAV2 capsid uses patches of positively charged amino acid residues to bind negatively charged HSPG on cell surfaces.<sup>19</sup> HSPG binding by AAV2 is the first important step in cellular transduction.<sup>23</sup> In our previous work aimed at building a provector prototype,<sup>17</sup> we hypothesized inserting negatively charged amino acids as part of the peptide lock would interfere with AAV2-HSPG interaction through an electrostatic repulsion mechanism. Indeed, our prior results show provectors in the locked state are poorly internalized by cells, and provector activation with MMPs dramatically enhances their cellular uptake.<sup>17</sup> Here, I

investigated whether our original hypothesis was correct or if amino acids with any chemical property may be used as the 4AA motif.

Using a random peptide library approach, Perabo et al. previously found that different 7-mer peptides have differential abilities to ablate HSPG binding when inserted in the HSPG binding domain of the AAV2 capsid.<sup>24</sup> Peptides with net positive charges were not effective in ablating binding. Conversely, peptides with net negative charges successfully ablated heparin binding. The authors suggested that peptide insertions in the heparin binding domain can affect HSPG interactions through different mechanisms that involve sterics and electrostatics.

On the basis of this prior work, it was feasible that either sterics or electrostatics could be driving the disruption of HSPG binding and cellular transduction by the 4AA motifs in the absence of MMPs. Surprisingly, almost all of the mutants, including the positively charged provector-K4 and provector-R4, display ablated heparin binding (**Figure 2-5**). Only the polar uncharged motifs retain marginal binding to heparin. We also observed that majority of the mutants are unable to transduce HEK293T cells in the absence of MMP, as desired (**Figure 2-6**). Again, only provector-N4, -Q4, and -SG2S retain any appreciable level of transduction ability. Due to issues with low viral production titers and inability to effectively lock the AAV capsid, most of the provector variants were not investigated further, leaving only provector-D4 and provector-E4 as viable design options. Finally, in the presence of MMP, provector-E4 behaves similarly to provector-D4 (**Figures**

## **2-7 and 2-8).**

During the course of the study, I observed unexpected results. The AAV2 capsid does not well-tolerate the insertion of positively charged 4AA motifs in the HSPG binding domain, as provector-K4 and provector-R4 display the lowest viral titers (**Figure 2-2**). In particular, provector-K4 displays an irregular Western blot pattern (**Figure 2-3**) and the capsid is unable to protect its genome effectively (**Figure 2-4**). provector-R4, on the other hand, has the lowest titer, but the capsid that does form is able to protect its genome similarly to wt (**Figure 2-4**).

Collectively, my data suggest that both electrostatic repulsion and steric obstruction between the 4AA motif and HSPG may make nonredundant contributions to the peptide lock being able to lock the capsid successfully. Negatively and positively charged motifs, and even small hydrophobic A4 and uncharged polar SG2S motifs, are able to lock the capsid, which would suggest steric obstruction plays an important role. However, the uncharged polar N4 and Q4 motifs, which are comparable in size to the D4 and E4 motifs but lacking negative charge, yield only partial ablation of receptor binding and cellular transduction, which may suggest that steric obstruction alone is not sufficient to block receptor binding. One potential explanation could be that the polar uncharged motif-containing peptide locks, although genetically inserted into the HSPG binding domain, do not assume the correct structural configuration to effectively block HSPG binding through sterics. Determining the structures of some of these provector variants

would likely shed light on the reasons for these experimental results. Differences in the amino acid sequence of the peptide insertion may account for the differing mechanisms behind the Perabo et al. report and the provector mutants described here.

Future work will address remaining unanswered questions about the provector design. First, structural studies must be performed to understand why peptide locks with four negatively charged amino acid residues are well-tolerated by the AAV capsid, whereas inserting virtually an identical lock (with the only difference being four positively charged residues) hinders capsid assembly and leads to poor capsid production. Furthermore, it is presently unclear if the 4AA motif is required at all, or exactly how many amino acid residues in the motif are needed to ablate cellular transduction. Additionally, an essential and universal cellular receptor for AAV infection, named AAVR, was recently discovered.<sup>25</sup> Whether the peptide locks interfere with AAVR binding by AAV2 remains to be determined. Lastly, creating provectors based on other AAV serotype capsids will reveal whether the uncovered design rules are broadly applicable to AAV-based provectors in general.

## **CONCLUSIONS**

The overall goal of this work was to investigate the role of the 4AA motif's chemical properties on provector function. Interestingly, I found motifs of various properties are able to lock the AAV2 capsid. However, due

to suboptimal production titers, potentially increased susceptibility to trypsin, and poor genome protection of majority of the mutants, the provector-E4 and provector-D4 variants appear to be the best design options so far. Continued investigation of the provector platform may further support the translation of this promising gene delivery technology for a variety of diseases characterized by elevated levels of extracellular proteases at target tissue sites. Center Vector Core for providing us with pXX2, pXX6-80, and scAAV2-CMV-GFP.

## **MATERIALS and METHODS**

### **Construction of provector Plasmids**

All provector plasmids were produced from pRC\_RR, a plasmid containing AAV serotype 2 (AAV2) rep and cap genes with NgoMIV and KasI sites at position 586 of cap.<sup>17</sup> provector plasmids containing various peptide locks were constructed by varying the tetra-amino acid motif of the inactivating domain. Oligonucleotides encoding the various locks were annealed and ligated into the NgoMIV and KasI sites in the pRC\_RR plasmid. provector variant plasmids (pPROVECTOR-D4, pPROVECTOR-E4, pPROVECTOR-K4, pPROVECTOR-R4, pPROVECTOR-A4, pPROVECTOR-N4, pPROVECTOR-Q4, pPROVECTOR-SG2S) were sequence-verified.

### **Virus Production**

Provector variants were produced through a triple plasmid cotransfection of (a) pXX6-80, a helper plasmid encoding adenoviral proteins; (b) pscGFP, self-complementary GFP transgene cassette; and (c) packaging plasmids encoding provector capsid derivatives.<sup>17</sup> Wild-type (wt) capsid AAV2 vector was produced through triple transfection of pXX6-80, pscGFP, and pXX2. Human Embryonic Kidney 293T cells (HEK 293T) were split 1:2 and plated on ten 15 cm plates (BD Falcon) coated with 0.001% poly-L-lysine (Sigma) 24h before transfection. 48 h post-transfection, the producer cells were harvested, pelleted, and resuspended in 1× Gradient Buffer (GB: 10 mM Tris, pH 7.6, 10 mM MgCl<sub>2</sub>, 150 mM NaCl). Cells were then lysed with three

freeze-thaw cycles followed by benzonase treatment (50 units/ml, Sigma) at 37 °C for 40 min. Cell lysate was centrifuged at 4 °C at 3,000g for 20 min and the supernatant was collected for iodixanol density gradient separation (Optiprep, Beckman Ultra-Clear QuickSeal Tubes). Samples were centrifuged at 18 °C at 48,000 rpm for 1h 45 min. Viruses were extracted from the 40% iodixanol layer and stored at 4 °C in 3 mL cryovials (Biotix). Viruses were purified with an anion exchange column (Pall Corporation) and concentrated with an amicon filter tube (Millipore) as published elsewhere.<sup>17</sup>

### **Quantification of Virus Titers**

Quantitative polymerase chain reaction (qPCR) was used to determine genomic viral titers as described elsewhere.<sup>20</sup> Briefly, viral titers were quantified using a C1000 thermal cycler (Bio-Rad) with SYBR green (Applied Biosystems) and primers against the CMV promoter (forward: 5'-TCACGGGGATTTCCAAGTCTC-3' and reverse: 5'-AATGGGGCGGAGTTGTTACGA-3').

### **Western Blotting and Silver Staining**

Western blot analysis was performed to detect viral capsid proteins. Samples were heat-denatured in LDS sample buffer and sample reducing agent (NuPAGE, Life Technologies) at 75 °C for 15 min. Denatured samples were loaded and separated via electrophoresis on a 4"12% Bis-Tris gel (NuPAGE, Life Technologies), transferred onto a nitrocellulose membrane, and probed sequentially with B1 primary antibody (American Research Products)

followed by horseradish peroxidase conjugated antimouse secondary antibody (American Research Products). Lumi-Light Western Blotting Substrate (Roche Applied Science) was then added to the nitrocellulose membrane and imaged with Fuji Las-4000.

Silver stain analysis was also conducted to detect viral capsid proteins as well as capsid proteolytic fragments. Viral samples were denatured in LDS and separated via electrophoresis on a 4"12% Bis- Tris gel (NuPAGE, Life Technologies). Viral capsid proteins and proteolytic fragments were detected with a silver stain kit according to manufacturer's protocol (Life Technologies, Carlsbad, CA).

### **Heparin Affinity Assay**

Provector mutants were tested for heparin binding ability. Viruses were added to heparin-agarose beads (Sigma H-6508) and incubated for 15 min at room temperature while continuously rotating. Samples were centrifuged for 5 min at 6000g and unbound fractions were collected. The beads were incubated sequentially with buffers containing increasing NaCl concentrations (300 mM, 500 mM, 700 mM, and 1 M) in order to elute heparin- bound viruses. All unbound and bound fractions were quantified for viral genome amounts via qPCR.

### **Nuclease Protection Assay**

Capsid stability of provector mutants was analyzed with a benzonase protection assay. Provector mutants were mixed with Endo buffer (1.5 mM

MgCl<sub>2</sub>, 0.5 mg/mL BSA, 50 mM Tris, pH 8.0) and incubated with benzonase nuclease (250 units/μL; Sigma) or sham buffer (50% glycerol, 50 mM Tris-HCl, pH 8.0, 20 mM NaCl, 2 mM MgCl<sub>2</sub>) at 37 °C for 30 min. Reactions were terminated with 0.5 M EDTA. Viral titers were then quantified with qPCR to calculate the percentage of protected viral genomes.

### **Cellular Transduction**

HEK293T cells were seeded on poly-L- lysine-coated 48-well plates at 1 × 10<sup>5</sup> cells/well. provector mutants were added to cells at a multiplicity of infection (MOI) of 500 and incubated in serum-free medium for 12 h.

Complete medium containing serum was added 12 h post-transduction. Cells were harvested 48 h post-transduction for flow cytometry with FACSCanto II flow cytometer (BD Biosciences).

### **Proteolysis**

Provector mutants were tested for MMP susceptibility. Protease activity was first calibrated with the fluorogenic substrate Mca-PLGL-Dpa-AR

(Calbiochem) at 5 nM enzyme and 5 μM substrate to determine initial enzyme velocities, as previously described.<sup>17</sup> Viruses were diluted in

reaction buffer (MMP Buffer: 50 mM Tris-Cl, pH 7.4, 150 mM NaCl, 5 mM

CaCl<sub>2</sub> and 1x GB- PF68). MMP-7 (Enzo Life Sciences, Farmingdale, NY) was

diluted in vehicle buffer (50 mM Tris, pH 7.5, 300 mM NaCl, 5 mM CaCl<sub>2</sub>, 10 μM ZnCl<sub>2</sub>, 0.5% Brij-35, 30% glycerol) and mixed with diluted virus.

Reactions were incubated at 37 °C for 12h and terminated with 50 mM

EDTA. For cellular transduction, MMP-treated viruses were added to HEK293T cells and incubated for 48 h. After 48 h, cells were harvested and analyzed with flow cytometry.

## REFERENCES

- (1) Egeblad, M.; Werb, Z. New functions for the matrix metalloproteinases in cancer progression. *Nat. Rev. Cancer* 2002, 2 (3), 161-74.
- (2) Thomas, C. V.; Coker, M. L.; Zellner, J. L.; Handy, J. R.; Crumbley, A. J., III; Spinale, F. G. Increased matrix metalloproteinase activity and selective upregulation in LV myocardium from patients with endstage dilated cardiomyopathy. *Circulation* 1998, 97 (17), 1708-15.
- (3) Gialeli, C.; Theocharis, A. D.; Karamanos, N. K. Roles of matrix metalloproteinases in cancer progression and their pharmacological targeting. *FEBS J.* 2011, 278 (1), 16-27.
- (4) Hadler-Olsen, E.; Winberg, J. O.; Uhlin-Hansen, L. Matrix metalloproteinases in cancer: their value as diagnostic and prognostic markers and therapeutic targets. *Tumor Biol.* 2013, 34 (4), 2041-51.
- (5) Roy, R.; Yang, J.; Moses, M. A. Matrix metalloproteinases as novel biomarkers and potential therapeutic targets in human cancer. *J. Clin. Oncol.* 2009, 27 (31), 5287-97.
- (6) Szarvas, T.; vom Dorp, F.; Ergun, S.; Rubben, H. Matrix metalloproteinases and their clinical relevance in urinary bladder cancer. *Nat. Rev. Urol.* 2011, 8 (5), 241-54.
- (7) Schulz, R. Intracellular targets of matrix metalloproteinase-2 in cardiac disease: rationale and therapeutic approaches. *Annu. Rev. Pharmacol.*

Toxicol. 2007, 47, 211-42.

(8) Wang, W.; Schulze, C. J.; Suarez-Pinzon, W. L.; Dyck, J. R.; Sawicki, G.; Schulz, R. Intracellular action of matrix metalloproteinase- 2 accounts for acute myocardial ischemia and reperfusion injury. *Circulation* 2002, 106 (12), 1543-1549.

(9) Ge, J.; Min, S. H.; Kim, D. H.; Lee, D. C.; Park, K. C.; Yeom, Y. I. Selective gene delivery to cancer cells secreting matrix metal- loproteinases using a gelatin/polyethylenimine/DNA complex. *Bio- technol. Bioprocess Eng.* 2012, 17 (1), 160-167.

(10) Gjetting, T.; Jolck, R. I.; Andresen, T. L. Effective nanoparticle- based gene delivery by a protease triggered charge switch. *Adv. Healthcare Mater.* 2014, 3 (7), 1107-18.

(11) Hartl, I.; Schneider, R. M.; Sun, Y.; Medvedovska, J.; Chadwick, M. P.; Russell, S. J.; Cichutek, K.; Buchholz, C. J. Library-based selection of retroviruses selectively spreading through matrix metal- loprotease-positive cells. *Gene Ther.* 2005, 12 (11), 918-26.

(12) Springfield, C.; von Messling, V.; Frenzke, M.; Ungerechts, G.; Buchholz, C. J.; Cattaneo, R. Oncolytic efficacy and enhanced safety of measles virus activated by tumor-secreted matrix metalloproteinases. *Cancer Res.* 2006, 66 (15), 7694-7700.

(13) Evans, A. C.; Thadani, N. N.; Suh, J. Biocomputing nanoplatfoms as

therapeutics and diagnostics. *J. Controlled Release* 2016, DOI:  
10.1016/j.jconrel.2016.01.045.

(14) Szecsi, J.; Drury, R.; Josserand, V.; Grange, M. P.; Boson, B.; Hartl, I.; Schneider, R.; Buchholz, C. J.; Coll, J. L.; Russell, S. J.; Cosset, F. L.; Verhoeven, E.; et al. Targeted retroviral vectors displaying a cleavage site-engineered hemagglutinin (HA) through HA-protease interactions. *Mol. Ther.* 2006, 14 (5), 735-44.

(15) Kotterman, M. A.; Schaffer, D. V. Engineering adeno-associated viruses for clinical gene therapy. *Nat. Rev. Genet.* 2014, 15 (7), 445-51.

(16) Santiago-Ortiz, J. L.; Schaffer, D. V. Adeno-associated virus (AAV) vectors in cancer gene therapy. *J. Controlled Release* 2016, DOI:  
10.1016/j.jconrel.2016.01.001.

(17) Judd, J.; Ho, M. L.; Tiwari, A.; Gomez, E. J.; Dempsey, C.; Van Vliet, K.; Igoshin, O. A.; Silberg, J. J.; Agbandje-McKenna, M.; Suh, J. Tunable Protease-Activatable Virus Nanonodes. *ACS Nano* 2014, 8 (5), 4740-4746.

(18) Ho, M. L.; Judd, J.; Kuypers, B. E.; Yamagami, M.; Wong, F. F.; Suh, J. Efficiency of Protease-Activatable Virus Nanonodes Tuned Through Incorporation of Wild-Type Capsid Subunits. *Cell. Mol. Bioeng.* 2014, 7 (3), 334-343.

(19) Opie, S. R.; Warrington, K. H., Jr.; Agbandje-McKenna, M.; Zolotukhin, S.; Muzyczka, N. Identification of amino acid residues in the capsid proteins

of adeno-associated virus type 2 that contribute to heparan sulfate proteoglycan binding. *Journal of virology* 2003, 77 (12), 6995-7006.

(20) Ho, M. L.; Adler, B. A.; Torre, M. L.; Silberg, J. J.; Suh, J. SCHEMA Computational Design of Virus Capsid Chimeras: Calibrating How Genome Packaging, Protection, and Transduction Correlate with Calculated Structural Disruption. *ACS Synth. Biol.* 2013, 2 (12), 724-733.

(21) Waley, S. G.; Watson, J. The action of trypsin on polylysine. *Biochem. J.* 1953, 55 (2), 328-37.

(22) Kaludov, N.; Brown, K. E.; Walters, R. W.; Zabner, J.; Chiorini, J. A. Adeno-associated virus serotype 4 (AAV4) and AAV5 both require sialic acid binding for hemagglutination and efficient transduction but differ in sialic acid linkage specificity. *Journal of virology* 2001, 75 (15), 6884-93.

(23) Summerford, C.; Samulski, R. J. Membrane-associated heparan sulfate proteoglycan is a receptor for adeno-associated virus type 2 virions. *J. Virol.* 1998, 72 (2), 1438-1445.

(24) Perabo, L.; Goldnau, D.; White, K.; Endell, J.; Boucas, J.; Humme, S.; Work, L. M.; Janicki, H.; Hallek, M.; Baker, A. H.; Buning, H. Heparan sulfate proteoglycan binding properties of adeno-associated virus retargeting mutants and consequences for their in vivo tropism. *J. Virol* 2006, 80 (14), 7265-9.

(25) Pillay, S.; Meyer, N. L.; Puschnik, A. S.; Davulcu, O.; Diep, J.;

Ishikawa, Y.; Jae, L. T.; Wosen, J. E.; Nagamine, C. M.; Chapman, M. S.;  
Carette, J. E. An essential receptor for adeno-associated virus infection.  
Nature 2016, 530 (7588), 108-12.

# **Chapter 3: Engineering Adeno-Associated Virus with a Self-Peptide for Immune Avoidance**

## **INTRODUCTION**

As a gene therapy vector, AAV offers several advantages of high persistence, broad tropism, and biosafety<sup>28</sup>. Unfortunately, activation of the humoral immune response by the virus capsid is a significant barrier for effective and widespread use in a clinical setting. AAV is a naturally occurring virus such that a wide span of the human population has anti-AAV antibodies that would neutralize or diminish transduction efficiency. Therefore, strategies are being developed to engineer “stealth” vectors that evade immune cells.

Antigen presenting cells (APCs) clear foreign substances from the body that are not recognized as “self” particles<sup>29</sup>. For example, macrophages phagocytose any foreign material: microorganisms, apoptotic cells, and pathogens. As a consequence, the delivery of therapeutic and imaging tools may be hindered because of rapid clearance from the circulatory system.

To tackle this problem, PEGylation became a popular stealthing strategy. But, it was discovered to elicit an immune response in the form of anti-PEG antibodies<sup>30</sup>. This will be problematic as people receive PEGlyated vectors during treatment over a period of time. Treatments will become progressively less efficacious due to increased immunogenicity. Other synthetic stealth polymers have been considered, but all of these methods

require chemical conjugation-poly-*N*-(2-hydroxypropyl) methacryamide (poly-HMPA), polysaccharides, and to the capsid that could decrease the efficiency or alter the tropism of vectors <sup>31</sup>. Thus, genetic insertion into rationally chosen capsid sites of a stealth peptide is a promising alternative to avoid detrimental conjugation methods.

CD-47, a membrane protein that is expressed on the surface of circulatory cells, is a potential biomolecule to explore as a stealthing strategy <sup>32</sup>. It is involved in the negative regulation of T-cell and humoral immune responses <sup>33</sup>. When circulatory cells encounter a macrophage, they use CD47 to bind to the SIRPα receptor located on the macrophage surface. The CD47 - SIRPα receptor binding interaction elicits a “Don’t Eat Me Signal”, allowing the CD-47 expressing cell to escape being engulfed by the macrophage <sup>29</sup>.

Rodriguez et al. investigated whether a synthetic Self Peptide (SP), a truncated form of CD47 can decrease phagocytic uptake of nanoparticles in cellular and animal models<sup>34</sup>. The researchers synthesized a SIRPα-binding bioactive region of CD47, a 21-amino acid named ‘self-peptide’, for attachment to virus-like nanobeads to prevent APC uptake. Conjugation of the SP to nanoparticles led to increased circulation time coupled with reduced macrophage phagocytic uptake <sup>34</sup>. Also, the CD47 concept was expanded to a lentiviral vectors <sup>35</sup>. To generate Lentivirus displaying CD47 (CD47-Lenti), HEK293T cells expressing CD47 were used for virus production. As observed for SP-conjugated nanoparticles, CD47-Lenti exhibited longer circulation time and less phagocytic susceptibility *in vitro*

*and in vivo.*

Based on these promising results by others, I hypothesize genetic attachment of the self-peptide (SP) to the AAV capsid should decrease its immunogenicity and enable repeat dosing of the vector. My research addresses the AAV humoral immune response that is a major limitation for repeat administration in gene therapy.

## RESULTS

### Synthesis of AAV-SP variants

I constructed several AAV-SP variants to determine whether self-peptide (SP) and linker insertions [L1 =  $(G_4S_1)_2$  and L2 =  $(G_4S_1)_4$ ] (**Figure 3-1**) cause deleterious effects on virus capsid assembly, genome packaging, and genome protection (**Figure 3-2**).

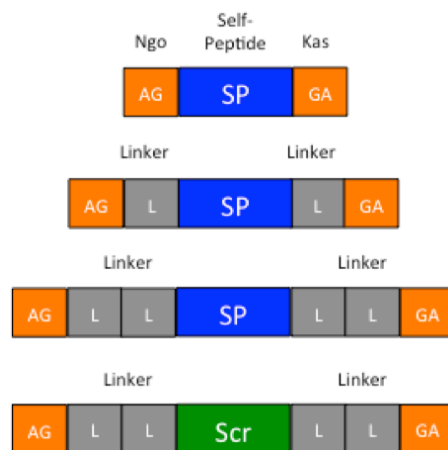


**Figure 3-1: Design of SP insertion into AAV capsid.** Self Peptide (SP) was inserted between restriction enzyme sites *NgoMIV* and *KasI*. Linkers (L1 or L2) flanked the SP insert. L1 =  $(G_4S_1)_2$  and L2 =  $(G_4S_1)_4$ .

I quantified titers of AAV-SP variants using a quantitative polymerase chain reaction (qPCR) assay (**Figure 3-2a**). The vectors with only SP

insertion (SP), decrease 1-log lower than wild-type (*wt*), which suggest that SP slightly decreases virus production.

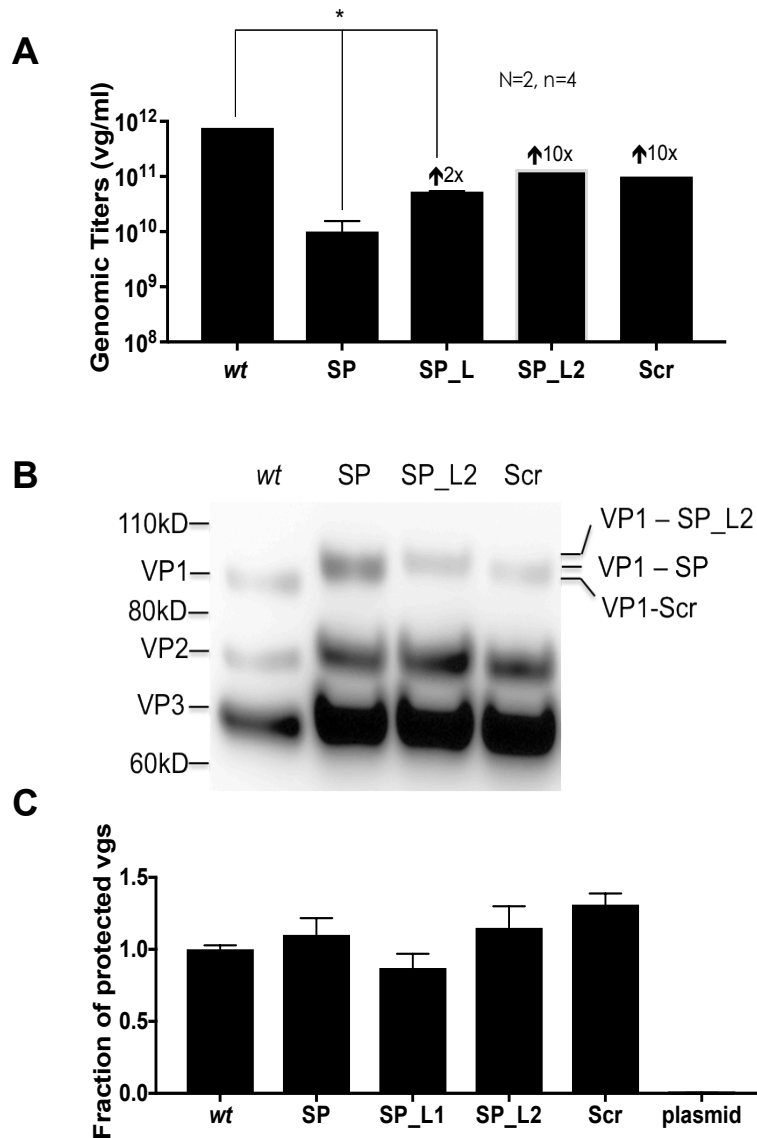


**Figure 3-2: Structural characterization of AAV-SP.** Genomic titers, VP band detection, and capsid stability were assessed. (a) qPCR was used to quantify viral titers (vg/ml). (b) A Western blot was performed to detect viral capsid proteins (VPs) and SP insertion in the AAV2 capsid. (c) Protected genomes were tested with a nuclease digestion and quantified with qPCR. For qPCR measurements, error bars represent SEM of two independent experiments conducted in duplicate. Asterisk indicates  $p < 0.05$  via ANOVA analysis.

Conversely, the SP with attached linkers (SP\_L , SP\_L2, Scr) demonstrated increased viral titers within 2-fold and 10-fold of *wt*,

respectively. This data suggests that the AAV capsid is most tolerant of SP insertion with additional linkers that likely relieve structural constraints during capsid assembly. To qualitatively detect viral capsid proteins (VPs) and SP incorporation into the capsid, I performed a Western Blot (**Figure 3-2b**). All AAV-SP mutants exhibit VP band patterns similar to *wt*, except with a distinct MW band shift due to peptide (SP) and linker insertion (SP\_L SP\_L2, Scr) in the VP! capsid. These results indicate the SP and linkers incorporate into the VP subunits and the subunits form the capsid. Lastly, I quantified whether the variants protect their packaged genomes using a nuclease protection assay (Figure 2c). Here, the variants are exposed to an external nuclease digestion (Figure 2c). All variants protect their encapsidated genomes similar to *wt* capsid. Collectively, the results show that self-peptide and linker insertion do not cause adverse structural effects in viral production and capsid stability.

### **Infectivity of AAV-SP variants**

Next, I studied the viral infectivity of the AAV2-SP variants (**Figure 3-3**). All of the variants (SP, SP\_L2, Scr) exhibit transduction efficiency similar to *wt*, with the exception of SP\_L1. As compared to *wt* capsid, SP\_L1 displays 2-fold decrease in transduction efficiency. Therefore, insertion of one set of linkers may impose structural constraints or barriers for viral infectivity such as HSPG binding, nuclear trafficking, or transgene release from the capsid. Further analysis of heparin binding as shown in figure 2-5 may elucidate the heparin-binding index of L1. Also, viral trafficking of L1 may be observed for subcellular compartmentalization, viral uncoating, and

transgene transcription to determine if any of these events may explain its defective infectivity levels. As noted in Chapter 4, these assays were implemented to study AAV intracellular trafficking. In sum, SP and L2 do not cause a significant impact in transduction efficiency.

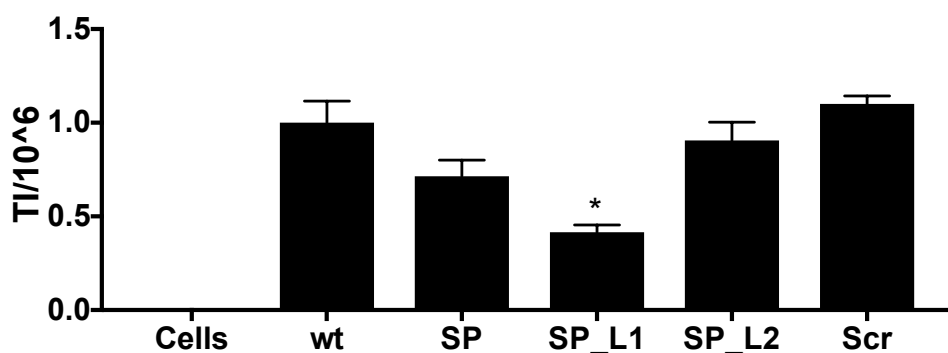


**Figure 3-3: Transduction of AAV-SP mutants.** AAV-SP mutants at a multiplicity of infection (MOI) of 1000 were added to HEK293T cells. Flow cytometry was used to the Transduction index (TI), which is a linear trend for viral transduction. Error bars represent SEM of two independent experiments conducted in duplicate. Asterisk indicates  $p < 0.05$  via ANOVA analysis.

### Phagocytic susceptibility of AAV-SP variants

To test for phagocytic susceptibility of AAV-SP variants, I quantified viral genome uptake in THP-1 cells (**Figure 3-4**). THP-1 monocytes were treated with PMA for macrophage differentiation. After 5 days, the macrophages were incubated with the viruses for 2 hours. Post incubation, the cells were harvested and lysed for DNA isolation. The eluted DNA concentration was measured with a nanodrop. The number of viral genomes in the DNA sample was then quantified using qPCR. As expected, *wt* and *Scr* show high levels of macrophage uptake. Interestingly, the other variants exhibited decreased macrophage uptake. Both SP and SP\_L2 display

decreased macrophage uptake by nearly 10-fold while SP\_L1 decreased closer to 4-fold when compared to *wt*. These findings indicate that SP and SP\_L2 insertion in the AAV2 capsid show the most dramatic decrease in phagocytosis among the mutant panel.

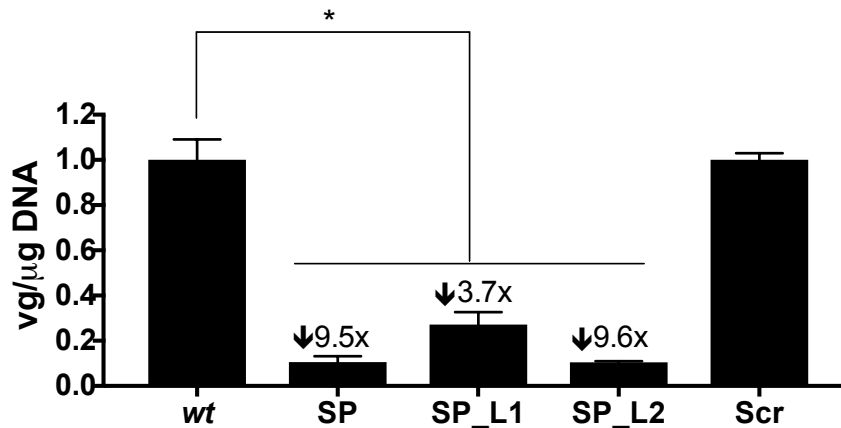


**Figure 3-4: Macrophage uptake of AAV-SP mutants.** AAV-SP mutants at a multiplicity of infection (MOI) of 1000 were added to THP-1 macrophages. Cells were harvested and lysed for DNA collection. To measure phagocytosed viruses, qPCR was used to quantify viral genomes (vgs) and normalized to DNA concentration ( $\mu\text{g DNA}$ ). Error bars represent SEM of two independent experiments conducted in duplicate. Asterisk indicates  $p < 0.05$  via ANOVA analysis.

### Phagocytic Susceptibility of SP\_L2 in non-SIRPa expressing cells

To determine whether SIRPa – SP signaling is responsible for decreased phagocytosis, THP-1 macrophages were treated with an anti- SIRPa antibody to knockdown SIRPa expression (Figure 3-5). After antibody treatment for 1 h, AAV-SP variants (SP\_L2 and Scr.SP\_L2) were added. As shown above, cells were processed for DNA isolation post incubation for 2 h. Furthermore, DNA was assayed for total concentration of DNA and viral genomes. In non-SIRPa-expressing THP-1 cells, the negative control, Scr-SP\_L2, showed phagocytic susceptibility as *wt*. I hypothesized that blocking

SIRP $\alpha$  binding to SP would allow the variants to undergo macrophage uptake. As expected, SP\_L2 regained phagocytic susceptibility. SP\_L2 displayed increased macrophage uptake similar to *wt* and Scr. Taken together, these findings demonstrate that SIRP $\alpha$  - SP signaling is the key mechanism for decreased phagocytic susceptibility.

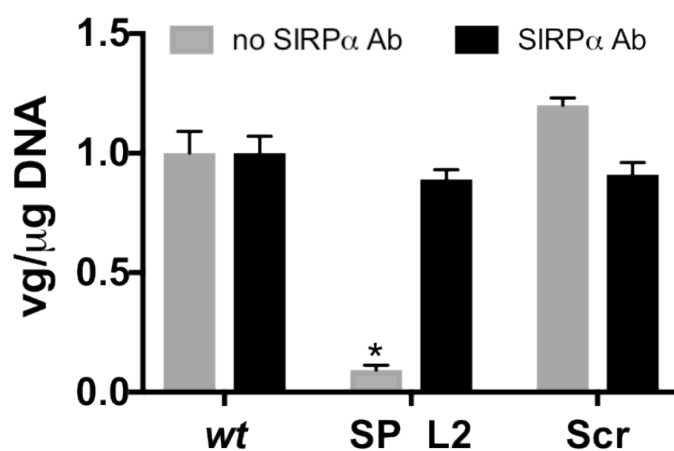


**Figure 3-5: Macrophage uptake of AAV-SP mutants in the presence of anti-SIRP $\alpha$ .** At MOI = 1000, SP\_L2 and Scr\_L2 variants were incubated in non-SIRP $\alpha$  expressing cells for 1 h. Post incubation, cells were collected for DNA analysis. To assess phagocytic recovery, qPCR was used to measure viral genomes (vgs) and normalized to DNA concentration ( $\mu$ g DNA). Error bars represent SEM of two independent experiments conducted in duplicate. Asterisk indicates  $p < 0.05$  via ANOVA analysis.

## DISCUSSION and CONCLUSIONS

From our previous work, we identified residue 453 as a region in the AAV2 capsid that can tolerate mCherry insertion without decreasing virus transduction efficiency<sup>36</sup>. Since mCherry is a 256 amino acid<sup>36</sup> protein, we hypothesize that insertion of a much smaller 21 aa CD-47 SP into the same position would be well-tolerated by the capsid. mCherry was also successfully displayed on the capsid surface; therefore, this suggests that SP will also

protrude from the capsid surface for binding interaction with the SIRP $\alpha$  receptor on macrophages.

As discussed previously, Discher's research group demonstrated exemplary success in the development of nanoparticles (synthetic and viral) that evade macrophage phagocytosis via CD47 signaling. Based on this prior work, we aimed to test this concept to generate an immune-evasive AAV vector. Promisingly, all the AAV-SP mutants exhibited decreased phagocytic susceptibility; however, SP\_L1 demonstrated the highest level of macrophage uptake among the mutant panel. Since SP\_L2 had the highest viral titers, I moved forward in this study with this variant. In the non-SIRP $\alpha$  expressing cells, SP\_L2 regained macrophage uptake as *wt* and the scrambled negative control (Scr). Collectively, my data suggest that SP insertion in the AAV2 capsid at position 453 hinders phagocytic uptake. In addition, linker insertion improves viral production, yet, the number of linkers impact SP functionality for macrophage interaction.

To assess whether SP:SIRP $\alpha$  signaling is responsible for decreased uptake, I conducted a knockdown assay of SIRP $\alpha$  to measure the number of engulfed viruses. The data demonstrates that the L2 mutant regains phagocytic susceptibility as *wt* and Scr. Therefore, the signaling mechanism between the SIRP $\alpha$  macrophage receptor and the SP moiety on the AAV2 capsid may be an explanation for the degree of macrophage uptake.

I have clearly demonstrated a proof-of-concept model of an AAV vector that can evade macrophage uptake. The major goal is to design and to construct a panel of AAV vectors that have a lower immunogenic profile and

decreased adaptive immune system activation. Hopefully, the long-term benefit of establishing an immune-evasive AAV vector platform may lead to therapeutic and cost effective gene medicine for a large number of disease indications.

Continued studies with an *in vivo* model should also be implemented to investigate NAb production from AAV-SP administration. More detailed analysis will further elucidate AAV-SP and APCs interaction *in vitro* and *in vivo*.

## **MATERIALS and METHODS**

### **Molecular Cloning of SP mutant plasmids**

To generate AAV2-SP, using a KasI and NgoMIV restriction digestion, mCherry was removed from the pRC\_RR\_VP1\_r1c3 construct (a plasmid encoding AAV2 rep and cap with mCherry inserted in position 453 of the VP1 capsid). Oligonucleotide encoding the SP sequence (GNYTCEVTELTREGETIIEELK)<sup>34</sup> was annealed and ligated into the NgoMIV and KasI sites in the pRC\_RR\_VP1\_r1c3 plasmid. All SP-inserted capsid genes were sequence-verified.

### **Synthesis of AAV-SP mutants**

The SP mutants were produced through a quadruple plasmid cotransfection of a) pXX6-80, a helper plasmid encoding adenoviral proteins; b) pscGFP, self-complementary GFP transgene cassette; c) packaging plasmid encoding VP1-SP subunit; and d) packaging plasmid encoding wt VP2 and VP3 subunits. Plasmids were transfected into Human Embryonic Kidney 293T cells (HEK 293T) to produce virus. The produced virus was extracted from HEK293T cells and separated with an iodixanol gradient and ultracentrifugation. Viruses were purified using amicon concentration.

### **Characterization of SP mutants**

Quantitative polymerase chain reaction (qPCR) was used to determine viral genomic titers. Briefly, viral titers were quantified with SYBR green and primers against the CMV promoter. Western blot analysis was performed to detect viral

capsid proteins (VP1, VP2, VP3) with a B1 antibody. To image the blot, a Fujifilm LAS 4000 with Lumi-Light Western blotting substrate was used to distinguish corresponding VP bands (Roche). To analyze capsid stability, AAV-SP mutants were incubated with a mixture of Endo buffer (1.5 mM MgCl<sub>2</sub>, 0.5 mg/mL BSA, 50 mM Tris, pH 8.0) and either benzonase nuclease (250 units/μL; Sigma) or sham buffer (50% glycerol, 50 mM Tris-HCl, pH 8.0, 20 mM NaCl, 2 mM MgCl<sub>2</sub>) at 37 °C for 30 min. To terminate the reaction, 0.5 M EDTA was added. qPCR was used to measure viral titers and to calculate the fraction of protected GFP genomes. For cellular transduction, HEK 293T cells were seeded in 48-well plates. Cells were transduced with AAV-SP vectors containing GFP transgene cassette at an MOI of 1,000 after 24 h. For 12 h, cells were incubated in a mixture of virus and serum-free media at 37 °C for 12h. To quantify GFP expression, cells were collected for flow cytometry (FACSCanto II) after 48 h. FlowJo software was used to analyze flow cytometry data and to calculate transduction index (TI).

### **Macrophage internalization assay of AAV-SP mutants.**

AAV-SP vectors at multiplicity of infection (MOIs) = 1000 were added to THP-1 macrophages treated with or without an anti-SIRPα antibody (Santa Cruz Biotechnology, SE7C2). After 2 h, macrophages were harvested and lysed for DNA collection with an E.Z.N.A Tissue DNA kit (Omega Bio-tek). The DNA concentration was measured with a nanodrop. Following DNA quantification, qPCR was conducted to quantify the number of viruses engulfed by macrophages.

## REFERENCES

- (1) Dunbar, C. E.; High, K. A.; Joung, J. K.; Kohn, D. B.; Ozawa, K.; Sadelain, M. Gene therapy comes of age. *Science* **2018**, *359*, eaan4672.
- (2) Jenks, S. Gene Therapy Death — "Everyone Has to Share in the Guilt". *JNCI: Journal of the National Cancer Institute* **2000**, *92*, 98-100.
- (3) Nienhuis, A. W.; Dunbar, C. E.; Sorrentino, B. P. Genotoxicity of retroviral integration in hematopoietic cells. *Mol Ther* **2006**, *13*, 1031-1049.
- (4) Cavazzana-Calvo, M., Hacein-Bey, S., de Saint Basile, G., Gross, F., Yvon, E., Nusbaum, P., Selz, F., Hue, C., Certain, S., Casanova, J.L. and Bouso, P., . Gene Therapy of human severe combined immunodeficiency (SCID)-X1 disease. *Science* **2000**, *288*, 669-672.
- (5) Wang, D.; Tai, P. W. L.; Gao, G. Adeno-associated virus vector as a platform for gene therapy delivery. *Nat Rev Drug Discov* **2019**, *1*.
- (6) Padron, E.; Bowman, V.; Kaludov, N.; Govindasamy, L.; Levy, H.; Nick, P.; McKenna, R.; Muzyczka, N.; Chiorini, J. A.; Baker, T. S.; Agbandje-McKenna, M. Structure of adeno-associated virus type 4. *J Virol* **2005**, *79*, 5047-5058.
- (7) Xie, Q.; Bu, W.; Bhatia, S.; Hare, J.; Somasundaram, T.; Azzi, A.; Chapman, M. S. The atomic structure of adeno-associated virus (AAV-2), a vector for human gene therapy. *Proc Natl Acad Sci U S A* **2002**, *99*, 10405-10410.
- (8) O'Donnell, J.; Taylor, K. A.; Chapman, M. S. Adeno-associated virus-2 and its primary cellular receptor--Cryo-EM structure of a heparin complex. *Virology* **2009**, *385*, 434-443.

- (9) Schmidt, M.; Govindasamy, L.; Afione, S.; Kaludov, N.; Agbandje-McKenna, M.; Chiorini, J. A. Molecular characterization of the heparin-dependent transduction domain on the capsid of a novel adeno-associated virus isolate, AAV(VR-942). *J Virol* **2008**, *82*, 8911-8916.
- (10) Florian Sonntag, K. S., and Jurgen A. Kleinschmidt. A viral assembly factor promotes AAV2 capsid formation in the nucleolus. *PNAS* **2010**, *107*, 10220-10225.
- (11) Kotin, R. M., Marcello Siniscalco, R. Jude Samulski, X. D. Zhu, Lynne Hunter, Catherine A. Laughlin, Susan McLaughlin, Nicholas Muzyczka, Marino Rocchi, and Kenneth I. Berns. . Site-specific integration by adeno-associated virus. *Proceedings of the National Academy of Sciences* **1990**, *87*, 2211-2215.
- (12) Pillay, S.; Meyer, N. L.; Puschnik, A. S.; Davulcu, O.; Diep, J.; Ishikawa, Y.; Jae, L. T.; Wosen, J. E.; Nagamine, C. M.; Chapman, M. S.; Carette, J. E. An essential receptor for adeno-associated virus infection. *Nature* **2016**, *530*, 108-112.
- (13) Wang, D.; Tai, P. W. L.; Gao, G. Adeno-associated virus vector as a platform for gene therapy delivery. *Nat Rev Drug Discov* **2019**.
- (14) Ferrari, F. K., Samulski, T., Shenk, T. and Samulski, R.J. Second-strand synthesis is a rate-limiting step for efficient transduction by recombinant adeno-associated virus vectors. *Journal of virology* **1996**, *70*, 3227-3234.
- (15) McCarty, D. M., Fu, H., Monahan, P.E., Toulson, C.E., Naik, P. and Samulski, R.J. Adeno-associated virus terminal repeat (TR) mutant

generates self-complementary vectors to overcome the rate-limiting step to transduction in vivo. *Gene therapy* **2003**, *10*, 2112.

(16) McCarty, D. M. Self-complementary AAV vectors; advances and applications. *Mol Ther* **2008**, *16*, 1648-1656.

(17) Calcedo, R.; Morizono, H.; Wang, L.; McCarter, R.; He, J.; Jones, D.; Batshaw, M. L.; Wilson, J. M. Adeno-associated virus antibody profiles in newborns, children, and adolescents. *Clin Vaccine Immunol* **2011**, *18*, 1586-1588.

(18) Sylvie Boutin, V. M., Philippe Veron, Christian Leborgne, Olivier Benveniste, Marie Françoise Montus, and Carole Masurier. Prevalence of Serum IgG and Neutralizing Factors Against Adeno-Associated Virus (AAV) Types 1, 2, 5, 6, 8, and 9 in the Healthy Population: Implications for Gene Therapy Using AAV Vectors. *HUMAN GENE THERAPY* **2010**, *21*, 704-712.

(19) Chen, C. L.; Jensen, R. L.; Schnepp, B. C.; Connell, M. J.; Shell, R.; Sferra, T. J.; Bartlett, J. S.; Clark, K. R.; Johnson, P. R. Molecular characterization of adeno-associated viruses infecting children. *J Virol* **2005**, *79*, 14781-14792.

(20) Calcedo, R.; Vandenberghe, L. H.; Gao, G.; Lin, J.; Wilson, J. M. Worldwide epidemiology of neutralizing antibodies to adeno-associated viruses. *J Infect Dis* **2009**, *199*, 381-390.

(21) Boutin, S., Monteilhet, V., Veron, P., Leborgne, C., Benveniste, O., Montus, M.F. and Masurier, C. Prevalence of serum IgG and neutralizing factors against adeno-associated virus (AAV) types 1, 2, 5, 6, 8, and 9 in the

healthy population: implications for gene therapy using AAV vectors. *Human gene therapy* **2010**, *21*, 704-712.

(22) Mingozi, F.; High, K. A. Immune responses to AAV vectors: overcoming barriers to successful gene therapy. *Blood* **2013**, *122*, 23-36.

(23) Nathwani, A. C., Tuddenham, E.G., Rangarajan, S., Rosales, C., McIntosh, J., Linch, D.C., Chowdary, P., Riddell, A., Pie, A.J., Harrington, C. and O'beirne, J. Adenovirus-associated virus vector-mediated gene transfer in hemophilia B. *New England Journal of Medicine* **2011**, *365*, 2357-2365.

(24) Caitlin M. Guenther, B. E. K., Michael T. Lam, Tawana M. Robinson, Julia Zhao, and Junghae Suh. Synthetic Virology: Engineering Viruses for Gene Delivery. *Wiley Interdisciplinary Reviews: Nanomedicine and Nanobiotechnology* **2014**, *6*, 548-558.

(25) Munch, R. C.; Janicki, H.; Volker, I.; Rasbach, A.; Hallek, M.; Buning, H.; Buchholz, C. J. Displaying high-affinity ligands on adeno-associated viral vectors enables tumor cell-specific and safe gene transfer. *Mol Ther* **2013**, *21*, 109-118.

(26) Buning, H.; Srivastava, A. Capsid Modifications for Targeting and Improving the Efficacy of AAV Vectors. *Mol Ther Methods Clin Dev* **2019**, *12*, 248-265.

(27) Zhong, L.; Zhao, W.; Wu, J.; Li, B.; Zolotukhin, S.; Govindasamy, L.; Agbandje-McKenna, M.; Srivastava, A. A Dual Role of EGFR Protein Tyrosine Kinase Signaling in Ubiquitination of AAV2 Capsids and Viral Second-strand DNA Synthesis. *Molecular Therapy* **2007**, *15*, 1323-1330.

- (28) Maersch, S.; Huber, A.; Buning, H.; Hallek, M.; Perabo, L. Optimization of stealth adeno-associated virus vectors by randomization of immunogenic epitopes. *Virology* **2010**, *397*, 167-175.
- (29) Subramanian, S.; Parthasarathy, R.; Sen, S.; Boder, E. T.; Discher, D. E. Species- and cell type-specific interactions between CD47 and human SIRPalpha. *Blood* **2006**, *107*, 2548-2556.
- (30) Taro Shimizu, M. I., Yasuo Yoshioka, Tatsuhiro Ishida, Shinsaku Nakagaw, and Hiroshi Kiwadaa. Intravenous Administration of Polyethylene Glycol-Coated (PEGylated) Proteins and PEGylated Adenovirus Elicits an Anti-PEG Immunoglobulin M Response. *Biol. Pharm. Bull.* **2012**, *35*, 1336–1342.
- (31) Bartel, M.; Schaffer, D.; Buning, H. Enhancing the Clinical Potential of AAV Vectors by Capsid Engineering to Evade Pre-Existing Immunity. *Front Microbiol* **2011**, *2*, 204.
- (32) Jaiswal, S.; Jamieson, C. H.; Pang, W. W.; Park, C. Y.; Chao, M. P.; Majeti, R.; Traver, D.; van Rooijen, N.; Weissman, I. L. CD47 is upregulated on circulating hematopoietic stem cells and leukemia cells to avoid phagocytosis. *Cell* **2009**, *138*, 271-285.
- (33) Bouguermouh, S.; Van, V. Q.; Martel, J.; Gautier, P.; Rubio, M.; Sarfati, M. CD47 Expression on T Cell Is a Self-Control Negative Regulator of Type 1 Immune Response. *The Journal of Immunology* **2008**, *180*, 8073-8082.
- (34) Rodriguez, P. L.; Harada, T.; Christian, D. A.; Pantano, D. A.; Tsai, R. K.; Discher, D. E. Minimal "Self" peptides that inhibit phagocytic

clearance and enhance delivery of nanoparticles. *Science* **2013**, 339, 971-975.

(35) Sosale, N. G.; Ivanovska, II; Tsai, R. K.; Swift, J.; Hsu, J. W.; Alvey, C. M.; Zoltick, P. W.; Discher, D. E. "Marker of Self" CD47 on lentiviral vectors decreases macrophage-mediated clearance and increases delivery to SIRPA-expressing lung carcinoma tumors. *Mol Ther Methods Clin Dev* **2016**, 3, 16080.

(36) Judd, J.; Wei, F.; Nguyen, P. Q.; Tartaglia, L. J.; Agbandje-McKenna, M.; Silberg, J. J.; Suh, J. Random Insertion of mCherry Into VP3 Domain of Adeno-associated Virus Yields Fluorescent Capsids With no Loss of Infectivity. *Mol Ther Nucleic Acids* **2012**, 1, e54.

# **Chapter 4: Investigation of an Essential Serine-Rich Motif for AAV Intracellular Trafficking to the Nucleus**

## **INTRODUCTION**

To date, AAV vectors have demonstrated safety and efficacy in 176 phase I, II, and III clinical trials involving nearly eight human diseases <sup>26</sup> . Despite these remarkable achievements, the full therapeutic potential of AAV vectors may be improved through capsid engineering to improve cell transduction efficiency. Efficient gene therapy is hindered by three major barriers at the cellular level: (i) receptor attachment and entry, <sup>35</sup> post entry trafficking, and (iii) nuclear import. Therefore, investigation of the AAV intracellular trafficking pathway may reveal ways to develop improved gene therapy vectors.

For AAV intracellular trafficking, AAV goes into the cell, escapes from the endosome, enters the nucleus, uncoats its capsid, and releases its transgene for expression. Within the AAV capsid, highly conserved functional domains have been identified to be essential for endosomal escape and nuclear localization, PLA2 domain and BR3, respectively <sup>37,38</sup> . Other amino acid residues have been discovered that determine AAV's trafficking route. Salganik et al. studied four interacting amino acids (E563, H526, R389, and Y704), noted as the pH quartet in AAV8 <sup>39</sup> . Vectors

mutated in these residues (E563A, H526A, R389A, and Y704A) showed that all produced titers similar to *wt*. Of the mutant panel, Y704A displayed an adverse transduction defect greater than 7-log while the others had minimal transduction defects. Since Y704A seemed to be essential for viral transduction, further studies were continued to elucidate its defective behavior. Surprisingly, Y704A displayed cell entry, nuclear trafficking, and viral uncoating phenotypes similar to *wt*. A possible explanation of impaired second-strand synthesis may be responsible for defects in transduction. mRNA levels of Y704A were reduced 450-fold, which suggests that this mutant failed to facilitate transgene transcription for efficient transduction. Collectively, the authors found that AAV capsids may modulate both second-strand synthesis and transcription of the transgene.

In addition, Aydemir et al. investigated other AAV2 mutants (D529A, K692A, D528A, and D564A) that exhibited impaired viral transduction correlated to transcription defects<sup>40</sup>. These mutants had cellular entry, subcellular fractionation and uncoated genomes similar to *wt*. Interestingly, transcribed genomes were 300-fold lower (D529A and K692A) or 5 logs lower (D528A and D564A) when compared to *wt*. Overall, these results indicate that diminished transcription is responsible for a significant decrease in transduction for certain capsid mutants.

Though some aspects of AAV intracellular trafficking is better understood, there are still gaps in explaining mechanisms that regulate the major processes such as viral trafficking through the cytoskeletal network,

nuclear uptake via the nuclear pore complex, and capsid uncoating to release the genome. Much is yet to be known for the function of amino acid residues and associated functional domains that play a key role in viral trafficking.

To uncover whether other potential amino acid residues may be essential for viral infection, we explored serine residues in the VP1/2 N-terminus of the AAV capsid. Since serine residues are the most common phosphorylated amino acids <sup>26</sup>, they may serve as critical participants in AAV trafficking. With this acquired insight, we may be able to tune viral characteristics for improvement in AAV-based gene delivery.

## **RESULTS**

### **Bioinformatic Alignment of N-Terminal S/T Motif in AAV VP1 and VP2 Subunits**

To analyze the conservation of residues D154, S155, S156, S157, and G158 in AAV2's VP1 and VP2 subunits, we conducted a multiple alignment of 140 sequences of AAV VP1 available on GenBank (accession numbers in **Supplemental Table S1**). G158 appears to be the most conserved across AAV variants with prevalence at 96.4% (**Figure 4-1**). D154, S155, and S156 all have frequencies above 90%. S157 displays the lowest conservation at 52.9%. The second most prevalent amino acid at position 157 is T at 40.7%. Overall, the DSSSG motif appears highly conserved amongst AAV variants.

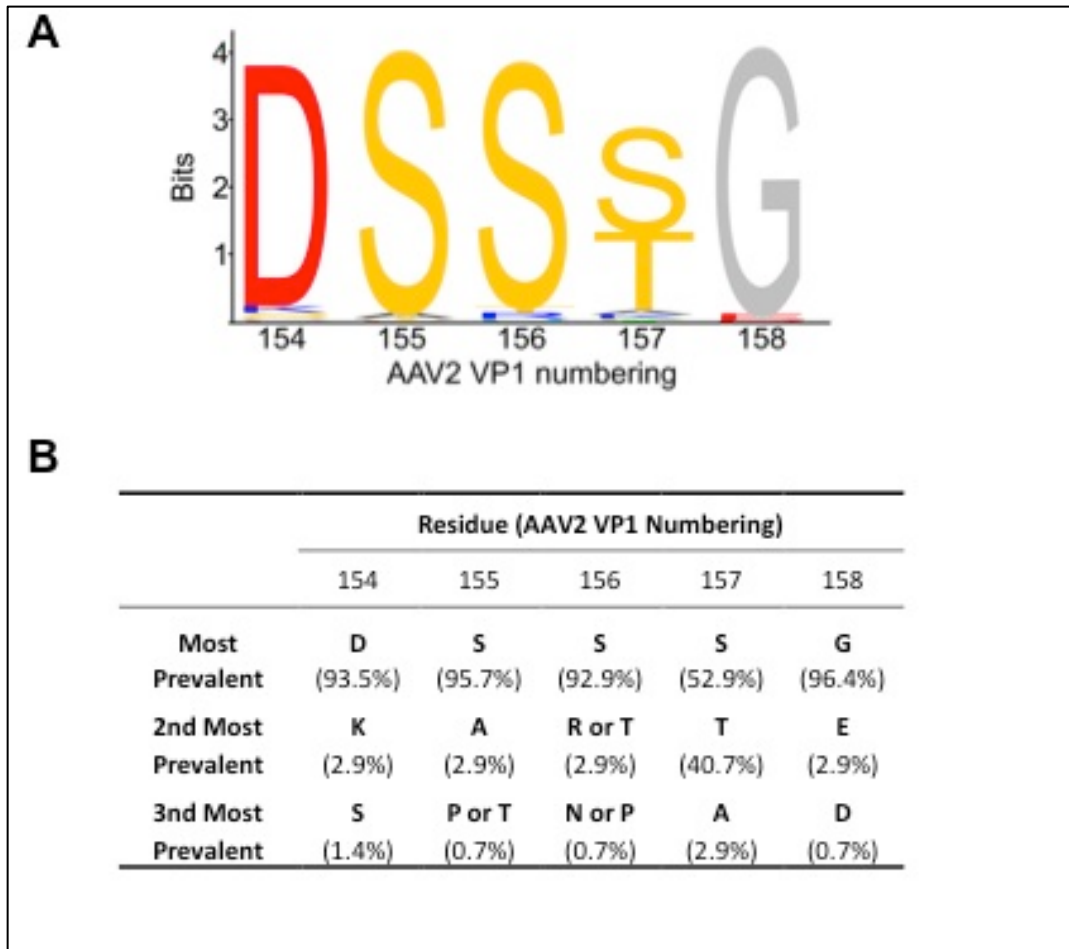


**Figure 4-1. Multiple sequence alignment of 167 AAV VP1 sequences.** (a) Sequence logo was used to investigate the conservation of D154, S155, S156, S157, and G158 residues of AAV2. The bit height profile measures the certainty and frequency levels for conservation of each residue. (b) Table 1 shows prevalence of D154, S155, S156, S157, and G158 residues of AAV2 according to percentage values.

## **Production of AAV2 Vectors with Alanine Substitutions in the N-Terminal S/T Motif**

We generated AAV2 capsid variants with amino acid residues within the N-terminal S/T motif mutated to alanine, and the resulting vectors were characterized for changes in capsid formation and genome protection ability. All mutant vector titers are statistically similar to those of the wt AAV2 capsid vector (**Figure 4-2a**). Therefore, alanine mutagenesis of this N-terminal S/T motif does not seem to disrupt viral assembly and genome packaging. We assessed viral capsid subunit incorporation via Western blot, whereby all mutants exhibit capsid compositions akin to that of *wt* capsid (**Figure 4-2b**). Finally, we performed a nuclease protection assay to quantify the abilities of the mutants to protect their genomes from external nuclease digestion (**Figure 4-2c**). All mutants display similar abilities to protect their encapsidated genomes as that of *wt* capsid. Our results demonstrate that alanine substitutions in the N-terminal S/T motif do not impact capsid formation, genome packaging, or genome protection.

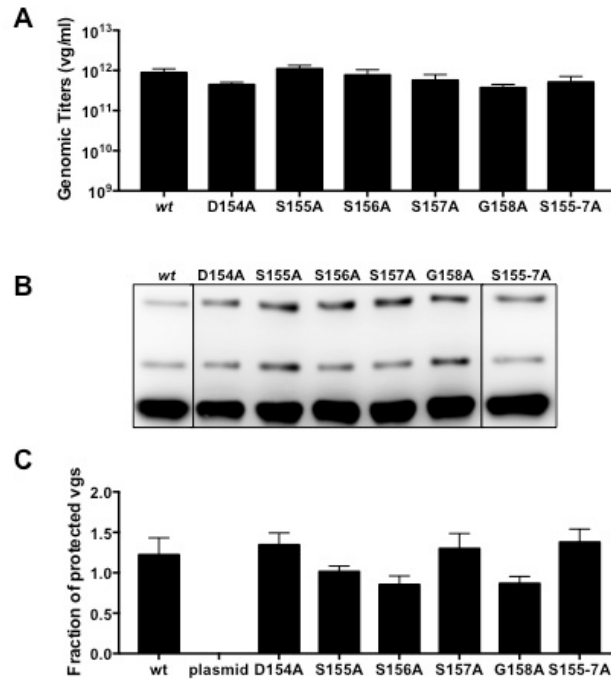


**Figure 4-2. Production of AAV2 vectors with alanine substitutions in the N-terminal S/T motif.** (a) Virus titers from two independent virus preparations were quantified using qPCR. Error bars represent SEM. (b) Same volume of iodixanol-purified virus was loaded per well. Capsid subunits were probed with the B1 antibody, which detects a C-terminal epitope shared among the VPs. All mutants display the expected VP1, VP2, and VP3 band patterns. (c) AAV2 alanine mutants were incubated with benzonase nuclease to quantify fraction of protected viral genomes (vgs) using qPCR. *wt* AAV2 capsid vector and naked plasmid DNA were included as controls. Error bars represent SEM of two independent experiments performed in duplicate.

### Transduction Efficiency of AAV2 N-Terminal S/T Motif Mutants

Next, I determined the transduction efficiencies of the alanine mutant panel (**Figure 4-3**). When compared to *wt* capsid, D154A, S155A, G158A, and S155-7A exhibit significantly decreased transduction efficiencies, while S157A shows behavior on par with *wt* in both HEK 293T and HeLa cells. D154A and G158A mutants display the most dramatic reductions in transduction – greater than 10-fold decrease compared to *wt*. Of the serine

mutants, S155A and S155-7A exhibit 9- and 15-fold decreases in HeLa cells, respectively, compared to that of *wt*. The S156A mutant shows approximately a 2-fold decrease in HeLa cells but not in HEK293T cells, implying there may be a cell type-dependence. The results thus far demonstrate that residues D154 and G158 are critical for viral transduction, and S155 may be the most essential residue of the serine triplet.

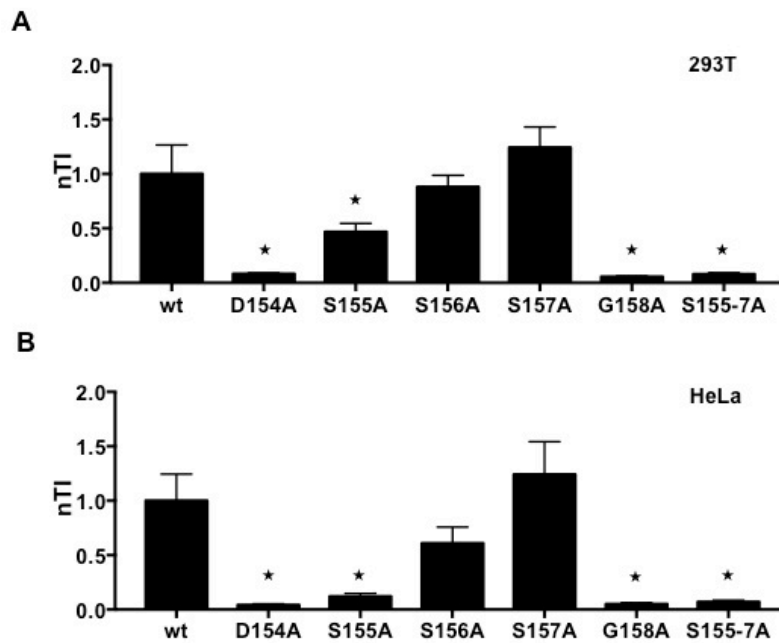


**Figure 4-3. Transduction efficiencies of AAV2 S/T motif mutants in HeLa and HEK293T cells.**

Vectors at a multiplicity of infection (MOI) of 500 were added to HEK293T and HeLa cells. Flow cytometry was conducted 48 h post-transduction. Transduction Index (TI) was calculated based on %GFP-positive cells multiplied by geometric mean fluorescence intensity. TI values were normalized to *wt* values. Error bars represent SEM of two independent experiments done in duplicate. Asterisk indicates  $p < 0.05$  by one-way ANOVA analysis.

## Cellular Internalization of AAV2 N-Terminal S/T Motif Mutants

To test for cellular uptake of the alanine mutant panel, I quantified viral genome internalization in HeLa cells (**Figure 4-4**). Cells were incubated with the viruses for 2 hours at which point cells were harvested, lysed, and DNA isolated from the samples. The number of viral genomes was then quantified using qPCR. Interestingly, all mutants internalize into cells similarly to *wt* capsid. These results suggest the N-terminal S/T motif does not play a role in cellular uptake of the vectors.

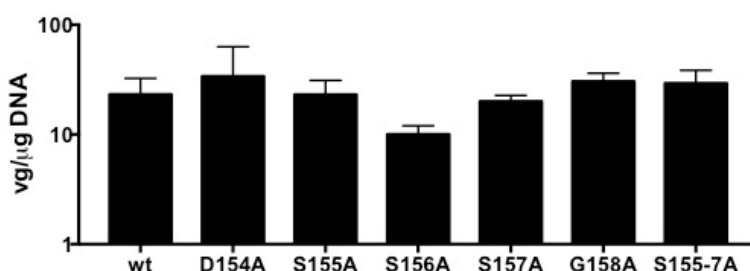


**Figure 4-4. Cellular uptake of AAV2 S/T motif mutants in HeLa cells.** Vectors at an MOI of 1000 were added to HeLa cells. Cells were harvested 24 h post-transduction and qPCR was used to quantify the number of internalized vgs normalized to total DNA content. Error bars represent SEM of two independent experiments done in duplicate.

## Nuclear Uptake of AAV2 N-Terminal S/T Motif Mutants

To assess nuclear uptake of the alanine mutants, I performed a subcellular fractionation and then quantified the number of viral genomes in the nucleus versus the cytoplasm of cells at 24 hours post-transduction (**Figure 4-5**). Comparison of absolute numbers of viral genomes reveals that all mutants are able to enter the nucleus as effectively as the *wt* capsid (**Figure 4-5a**). All viruses display similar levels of compartmentalization

between the nucleus and cytoplasm, with slightly more than half of the viral genomes located in the cytoplasm (**Figure 4-5b**). Taking the cellular internalization and subcellular fractionation results together, these mutants do not have significant differences in cellular levels in comparison to *wt*.

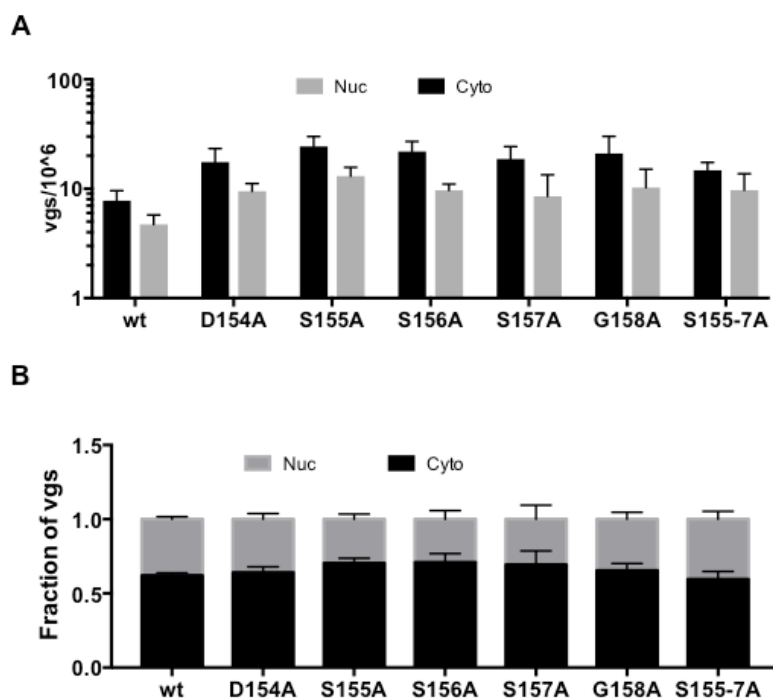


**Figure 4-5. Nuclear uptake of AAV2 S/T motif mutants in HeLa cells.** Vectors at an MOI of 1000 were added to HeLa cells, and cells were harvested 24 h post-transduction. After harvest, cytoplasmic and nuclear extracts were isolated for quantification of DNA. (a) qPCR was used to quantify the number of vgs in the cytoplasm versus the nucleus and then normalized to total DNA content measured with a nanodrop. (b) Intracellular viral genomes represented as fraction in the cytoplasm and nucleus. Error bars represent SEM of two independent experiments done in duplicate.

### Nuclear Uncoating of AAV2 N-Terminal S/T Motif Mutants

To determine nuclear uncoating of the alanine mutants, I conducted a nuclear uptake study as shown above. Benzonase-treated nuclear extracts were then quantified for the number of viral genomes at 24 hours post-transduction (**Figure 4-6a**). The absolute numbers of viral genomes showed

that only S157A exhibited nuclear uncoating as *wt*. Conversely, the remaining mutants (D154A, S155A, S156A, G158A, S155-7A) displayed abnormal results in nuclear uncoating (**Figure 4-6b**). From the mutant panel, the number of viral genomes appears to be larger than untreated samples. Due to these abnormalities, this data is not fully conclusive. However, nuclear capsid uncoating may likely be a cause for defective transduction efficiencies of the mutants.

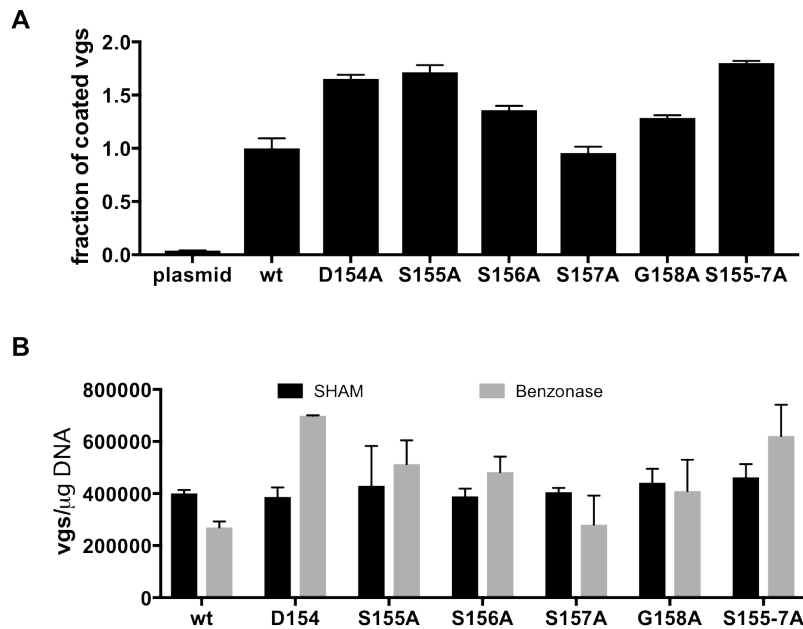


**Figure 4-6. Nuclear capsid uncoating of AAV2 S/T motif mutants in HeLa cells.** Vectors at an MOI of 1000 were added to HeLa cells, and cells were harvested 24 h post-transduction. After harvest, cytoplasmic and nuclear extracts were isolated for quantification of DNA. Total DNA content was measured with a nanodrop. qPCR was then used to quantify the number of vgs in the nuclear extracts for sham- and benzonase- treated samples. Error bars represent SEM of two independent experiments done in duplicate.

## Transcriptional Levels of AAV2 N-Terminal S/T Motif Mutants

Following the nuclear uncoating assay, I measured GFP mRNA expression levels by reverse transcribing isolated cellular mRNA (**Figure 4-7**). All mutants show defective GFP mRNA expression. Of the mutant panel, S157A retains the highest level of GFP mRNA expression close to *wt* levels. For the remaining serine mutants, S155A, S156A, and S155-7A, GFP mRNA expression is decreased close to 5-fold, while the flanking residue mutants, D154A and G158A display the most dramatic decrease at 9-fold when compared to *wt*. Considering the nuclear uncoating and mRNA transcription data, these results suggest that defects in viral capsid uncoating impact GFP mRNA expression which then leads to diminished transduction efficiency of the mutants.

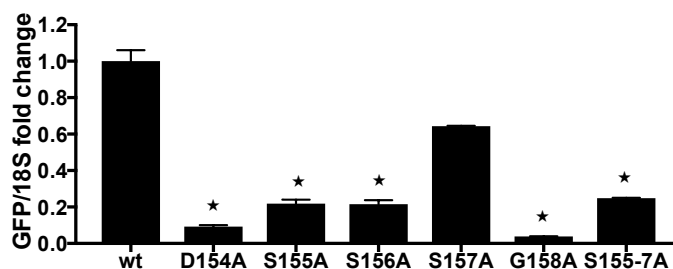


**Figure 4-7. GFP mRNA expression levels of AAV2 S/T motif mutants.** Vectors at an MOI of 1000 were added to HeLa cells, and cells were harvested 48 h post-transduction. After harvest, RNA was extracted and reverse transcribed into cDNA. qPCR was used to measure the relative GFP mRNA expression of the mutants relative to *wt* AAV2 capsid. Error bars represent SEM of four independent experiments done in duplicate. Asterisk indicates  $p < 0.05$  by one-way ANOVA analysis.

## DISCUSSION AND CONCLUSIONS

Alanine screening mutagenesis of a triple serine motif and its flanking residues has uncovered essential amino acids that are necessary for

transduction. Most of the mutants (D154A, S155A, S156A, S155-7A, and G158A) with the exception of S157A had a decrease in transduction efficiency. For the above analysis, major defects in nuclear uncoating and/or genome transcription may explain the diminished transduction efficiency. As discussed above, abnormalities in higher vg levels will need to be addressed via optimization strategies. One possible method is to stabilize the uncoated (free) viral genomes in the nuclear extract. Furthermore, among the mutant panel, D154A, S155A, and G158A appear to be the most defective mutants in transduction, nuclear uncoating, and genome transcription. Currently, the biological mechanism of these defects is unknown.

Though much is to be learned about the mechanistic processes involving serine/threonine/tyrosine capsid residues, some studies have been conducted to understand their critical role in AAV intracellular transport. In earlier studies, AAV nucleolar trafficking has been suggested to modulate transgene expression <sup>41</sup>. Thus, AAV nuclear location may affect viral infectivity. Other groups have discovered cellular proteins, such as FKBP52, a phosphatase that mediates dephosphorylation of serine/threonine residues, to be important for AAV transduction. Zhao et al. found that both cytosolic and nuclear FKBP52 attaches to the D-sequence of AAV ITRs to participate in AAV intracellular trafficking. Cytosolic FKBP52 facilitates AAV cellular transport and nuclear FKBP52 inhibits second-strand synthesis <sup>42</sup>. Cellular proteins may participate in unwanted attachment to the transgene cassette thus hindering genome transcription. Another question to explore is

whether the mutations studied in this project prevent cellular proteins from binding to the capsid, inhibiting important intracellular trafficking mechanisms. As a result, AAV may be more susceptible to degradation pathways – ubiquitination and proteasomal machinery – therefore, transduction efficiency is negatively impacted <sup>41,43,44</sup>.

In conclusion, we have found several amino acid residues in the N-terminus of the VP1/2 capsid subunit that are essential for AAV infectivity. Mechanistic studies should be implemented to gain a better understanding of AAV trafficking events: nucleolar location, binding cellular proteins, and post-translational modifications. For post-translational modifications, phosphorylation events appear to impact AAV's fate in the intracellular pathway <sup>41,44,45</sup>. However, putative sites for N- and O-linked glycosylation within the VP1/2 region of the AAV capsid have been found. For example, SGXG and SGLG motifs were identified at positions 157 and 195, respectively <sup>46</sup>. Continued research will broaden our understanding of AAV biology for future applications. Examples include studying phosphorylation with spectrometric methods, mutating serines in other AAV serotypes, and testing serine-based mutants *in vivo* for observation of transduction effects.

## **MATERIALS and METHODS**

### **Mutant Capsid Gene Cloning**

All AAV2 capsid mutants were created using the QuikChange Site-Directed Mutagenesis Kit (Agilent) to modify pXX2, a plasmid containing AAV serotype 2 (AAV2) *rep* and *cap* genes. Specifically, alanine scanning mutagenesis was performed on AAV2 capsid amino acid residues 148-161. All mutant capsid genes were sequence-verified by an external vendor (Genewiz).

### **Cell Culture**

HeLa and HEK 293T cells were maintained in Dulbecco's Modified Eagle Medium (DMEM, Life Technologies) supplemented with 10% fetal bovine serum (FBS, Atlanta-Biologicals) and 1% penicillin and streptomycin (Life Technologies). Cells were cultured at 37°C in 5% CO<sub>2</sub>.

### **Virus Production**

Viruses were generated through a triple plasmid co-transfection of HEK 293T cells with pscGFP (self-complementary GFP transgene flanked with AAV2 ITRs), pXX6-80 (adenoviral helper genes), and a plasmid encoding AAV2 *rep* and either wild type (wt) AAV2 *cap* or a mutated AAV2 *cap* gene. The HEK293T producer cells were seeded in 15cm dishes pre-coated with poly-L-lysine 24h before transfection at around 70-80% confluency. Cells were harvested 48h post-transfection, resuspended in media, transferred to a 50mL conical tube, and centrifuged at 1000xg for 15min at 4°C. After aspirating the supernatant, each pellet was then re-suspended in 13ml 1x

gradient buffer (GB: 10 mM MgCl<sub>2</sub>, 150 mM NaCl, 10 mM Tris, pH 7.6). Cell lysate was stored at -80°C until virus separation.

Frozen cell lysate was thawed in a 37°C water bath then snap frozen in liquid nitrogen twice for a total of three thaws. 2.5µL benzonase nuclease (250 units/µL; Sigma) was added to the thawed solution, which was then incubated for 40min in a 37°C water bath. The solution was then centrifuged at 3000xg for 20min at 4°C, and the supernatant was subsequently collected for iodixanol density gradient separation (Optiprep, Beckman Beckman #344326, Quick-Seal Ultra Clear 25 x 89 mm centrifuge tubes). Samples were then sealed and centrifuged at 48,000rpm for 1h 45min at 18°C. Viruses were extracted from the 40% iodixanol layer and stored at 4°C.

### **Quantification of Virus Titers**

Genomic viral titers were determined using qPCR. Samples were denatured by adding 10µl 2M NaOH to 10µl of virus and incubated at 75 °C for 30min, then neutralized with 10µl 2M HCl. 10µl of the resulting mixture was then combined with 490µl filler DNA [10ng/µl sheared salmon sperm DNA (Thermo Fisher Scientific) in UltraPure H<sub>2</sub>O]. Viral titers were quantified with SYBR green (Applied Biosystems) using C1000 thermal cycler (Bio-Rad) and primers against the CMV promoter (forward: 5'-TCACGGGGATTTCCAAGTCTC-3' and reverse: 5'-AATGGGGCGGAGTTGTTACGA-3').

## **Western Blot**

Viruses were run on a 7% Tris-Acetate gel (Life Technologies) and transferred to nitrocellulose (GE Healthcare) at 30V for 90 min. Blocking was performed in 5% skim milk in phosphate-buffer saline (PBS) with 0.1% Tween-20 (PBS-T) for 1h while rocking. Blots were then rinsed three times and rocked for 20min in PBS-T. Primary antibody B1 (monoclonal mouse anti-VPs, American Research Products, diluted 1:50) was applied to blots overnight at 4°C in PBS with 3% BSA (3% BSA-PBS). After washing with PBS-T, goat anti-mouse peroxidase-conjugated secondary antibody (Jackson ImmunoResearch) was applied at a 1:2000 dilution in 5% skim milk in PBS-T for 1h. Blots were then washed three times for 15min with PBS-T while rocking. Imaging was performed on a Fujifilm LAS 4000 with Lumi-Light Western blotting substrate (Roche).

## **Cellular Internalization Assay**

HEK 293T cells were seeded in 48-well plates. At 90% confluency, cells were transduced with virus at MOI of 1,000 for 2h at 37°C. 2h post-transduction, cells were then trypsinized and collected for DNA isolation and quantification. Total cell DNA was isolated using E.Z.N.A Tissue DNA kit (Omega Bio-tek), and DNA concentration was quantified with a Nanodrop spectrophotometer. qPCR was performed to quantify the number of viral genomes in each sample. Viral genomes per  $\mu\text{g}$  of total DNA was then calculated.

### **Subcellular Fractionation Assay**

HeLa cells were seeded in 6-well plates and pulse-transduced at 90% confluency at MOI 1000. Cells were transduced with AAV2 viruses encoding GFP at 4 °C for 30min. Cells were washed gently with cold PBS and incubated at 37 °C. 24h post-transduction, cells were harvested by trypsinization. Cytoplasmic and nuclear fractions were separated using a NE-PER Nuclear and Cytoplasmic Extraction Reagent kit (Thermo Scientific). Both fractions were subsequently incubated in PB buffer (Qiagen) containing 3M NaOAc for 10min at room temperature. Samples were purified using a QiaQuick Purification kit (Qiagen). Viral genomes in each sample were quantified using qPCR.

### **Nuclear Uncoating Assay**

HeLa cells were seeded in 6-well plates and pulse-transduced at 90% confluency at MOI 1000. Cells were transduced with AAV2 viruses encoding GFP at 4 °C for 30min. Cells were washed gently with cold PBS and incubated at 37 °C. 24h post-transduction, cells were harvested by trypsinization. Cytoplasmic and nuclear fractions were separated using a NE-PER Nuclear and Cytoplasmic Extraction Reagent kit (Thermo Scientific). The nuclear fractions were treated with either sham or benzoanase for 1 h (Sigma Aldrich). Both sham and benzoanase – treated samples were subsequently incubated in PB buffer (Qiagen) containing 3M NaOAc for 10min at room temperature. Samples were purified using a QiaQuick Purification kit (Qiagen). Viral genomes in each sample were quantified using qPCR against

the GFP transgene (forward primer TGA TGC CAC ATA CGG AAA GC and reverse primer AAA AGC ACT GCA CGC CAT AG).

### **Cellular Transduction Assay**

HEK 293T and HeLa cells were seeded in 48- or 12-well plates. After 24h, cells were transduced with AAV2 encoding GFP at an MOI of 1,000. Cells were incubated in virus-containing, serum-free media at 37°C for 12h. 48h post-transduction, cells were harvested for flow cytometry (FACSCanto II) to measure GFP expression. Flow cytometry data were analyzed using FlowJo software, and transduction efficiency was measured by calculating the transduction index (TI).

### **Nuclease Protection Assay**

5µl of virus sample was added to 45µl of Endo Buffer (1.5 mM MgCl<sub>2</sub>, 0.5 mg/mL BSA, 50 mM Tris, pH 8.0) and mixed well by inversion. 20µl of sample was aliquoted into two PCR tubes, one control and one to be treated with benzonase nuclease (250 units/µL; Sigma). 0.5µl of vehicle control was added to one tube and 0.5µl of benzonase to the other, mixed well by inversion, then collected by brief spin and incubated at 37°C for 30min. 0.5µl of 0.5M EDTA was then added to each tube to neutralize the enzyme. Viral genomes in each sample were quantified using qPCR.

### **RT-PCR assay**

HeLa cells were seeded in 6-well plates 24 h prior transduction. Cells were transduced with AAV2 virus encoding GFP at MOI of 1000. At 48 h post-transduction, cells were harvested and total RNA was measured with a

nanodrop (Qiagen). RNA samples were transcribed to cDNA using a Verso cDNA kit (Thermo Scientific). Real-time PCR (Bio-Rad) was used to quantify GFP transcripts with primers against the GFP transgene (forward primer TGA TGC CAC ATA CGG AAA GC and reverse primer AAA AGC ACT GCA CGC CAT AG). The housekeeping gene, 18S, was used to normalize the gene expression. GFP fold expression was compared to *wt* for absolute quantification.

## REFERENCES

- (1) Dunbar, C. E.; High, K. A.; Joung, J. K.; Kohn, D. B.; Ozawa, K.; Sadelain, M. Gene therapy comes of age. *Science* **2018**, *359*, eaan4672.
- (2) Jenks, S. Gene Therapy Death — "Everyone Has to Share in the Guilt". *JNCI: Journal of the National Cancer Institute* **2000**, *92*, 98-100.
- (3) Nienhuis, A. W.; Dunbar, C. E.; Sorrentino, B. P. Genotoxicity of retroviral integration in hematopoietic cells. *Mol Ther* **2006**, *13*, 1031-1049.
- (4) Cavazzana-Calvo, M., Hacein-Bey, S., de Saint Basile, G., Gross, F., Yvon, E., Nusbaum, P., Selz, F., Hue, C., Certain, S., Casanova, J.L. and Bousso, P., . Gene Therapy of human severe combined immunodeficiency (SCID)-X1 disease. *Science* **2000**, *288*, 669-672.
- (5) Wang, D.; Tai, P. W. L.; Gao, G. Adeno-associated virus vector as a platform for gene therapy delivery. *Nat Rev Drug Discov* **2019**, *1*.
- (6) Padron, E.; Bowman, V.; Kaludov, N.; Govindasamy, L.; Levy, H.; Nick, P.; McKenna, R.; Muzyczka, N.; Chiorini, J. A.; Baker, T. S.; Agbandje-McKenna, M. Structure of adeno-associated virus type 4. *J Virol* **2005**, *79*, 5047-5058.
- (7) Xie, Q.; Bu, W.; Bhatia, S.; Hare, J.; Somasundaram, T.; Azzi, A.; Chapman, M. S. The atomic structure of adeno-associated virus (AAV-2), a vector for human gene therapy. *Proc Natl Acad Sci U S A* **2002**, *99*, 10405-10410.

(8) O'Donnell, J.; Taylor, K. A.; Chapman, M. S. Adeno-associated virus-2 and its primary cellular receptor--Cryo-EM structure of a heparin complex. *Virology* **2009**, *385*, 434-443.

(9) Schmidt, M.; Govindasamy, L.; Afione, S.; Kaludov, N.; Agbandje-McKenna, M.; Chiorini, J. A. Molecular characterization of the heparin-dependent transduction domain on the capsid of a novel adeno-associated virus isolate, AAV(VR-942). *J Virol* **2008**, *82*, 8911-8916.

(10) Florian Sonntag, K. S., and Jurgen A. Kleinschmidt. A viral assembly factor promotes AAV2 capsid formation in the nucleolus. *PNAS* **2010**, *107*, 10220-10225.

(11) Kotin, R. M., Marcello Siniscalco, R. Jude Samulski, X. D. Zhu, Lynne Hunter, Catherine A. Laughlin, Susan McLaughlin, Nicholas Muzyczka, Marino Rocchi, and Kenneth I. Berns. . Site-specific integration by adeno-associated virus. *Proceedings of the National Academy of Sciences* **1990**, *87*, 2211-2215.

(12) Pillay, S.; Meyer, N. L.; Puschnik, A. S.; Davulcu, O.; Diep, J.; Ishikawa, Y.; Jae, L. T.; Wosen, J. E.; Nagamine, C. M.; Chapman, M. S.; Carette, J. E. An essential receptor for adeno-associated virus infection. *Nature* **2016**, *530*, 108-112.

(13) Wang, D.; Tai, P. W. L.; Gao, G. Adeno-associated virus vector as a platform for gene therapy delivery. *Nat Rev Drug Discov* **2019**.

(14) Ferrari, F. K., Samulski, T., Shenk, T. and Samulski, R.J. Second-strand synthesis is a rate-limiting step for efficient transduction by

recombinant adeno-associated virus vectors. *Journal of virology* **1996**, *70*, 3227-3234.

(15) McCarty, D. M., Fu, H., Monahan, P.E., Toulson, C.E., Naik, P. and Samulski, R.J. Adeno-associated virus terminal repeat (TR) mutant generates self-complementary vectors to overcome the rate-limiting step to transduction in vivo. *Gene therapy* **2003**, *10*, 2112.

(16) McCarty, D. M. Self-complementary AAV vectors; advances and applications. *Mol Ther* **2008**, *16*, 1648-1656.

(17) Calcedo, R.; Morizono, H.; Wang, L.; McCarter, R.; He, J.; Jones, D.; Batshaw, M. L.; Wilson, J. M. Adeno-associated virus antibody profiles in newborns, children, and adolescents. *Clin Vaccine Immunol* **2011**, *18*, 1586-1588.

(18) Sylvie Boutin, V. M., Philippe Veron, Christian Leborgne, Olivier Benveniste, Marie Françoise Montus, and Carole Masurier. Prevalence of Serum IgG and Neutralizing Factors Against Adeno-Associated Virus (AAV) Types 1, 2, 5, 6, 8, and 9 in the Healthy Population: Implications for Gene Therapy Using AAV Vectors. *HUMAN GENE THERAPY* **2010**, *21*, 704-712.

(19) Chen, C. L.; Jensen, R. L.; Schnepp, B. C.; Connell, M. J.; Shell, R.; Sferra, T. J.; Bartlett, J. S.; Clark, K. R.; Johnson, P. R. Molecular characterization of adeno-associated viruses infecting children. *J Virol* **2005**, *79*, 14781-14792.

(20) Calcedo, R.; Vandenberghe, L. H.; Gao, G.; Lin, J.; Wilson, J. M. Worldwide epidemiology of neutralizing antibodies to adeno-associated viruses. *J Infect Dis* **2009**, *199*, 381-390.

(21) Boutin, S., Monteilhet, V., Veron, P., Leborgne, C., Benveniste, O., Montus, M.F. and Masurier, C. Prevalence of serum IgG and neutralizing factors against adeno-associated virus (AAV) types 1, 2, 5, 6, 8, and 9 in the healthy population: implications for gene therapy using AAV vectors. *Human gene therapy* **2010**, *21*, 704-712.

(22) Mingozi, F.; High, K. A. Immune responses to AAV vectors: overcoming barriers to successful gene therapy. *Blood* **2013**, *122*, 23-36.

(23) Nathwani, A. C., Tuddenham, E.G., Rangarajan, S., Rosales, C., McIntosh, J., Linch, D.C., Chowdary, P., Riddell, A., Pie, A.J., Harrington, C. and O'beirne, J. Adenovirus-associated virus vector-mediated gene transfer in hemophilia B. *New England Journal of Medicine* **2011**, *365*, 2357-2365.

(24) Caitlin M. Guenther, B. E. K., Michael T. Lam, Tawana M. Robinson, Julia Zhao, and Junghae Suh. Synthetic Virology: Engineering Viruses for Gene Delivery. *Wiley Interdisciplinary Reviews: Nanomedicine and Nanobiotechnology* **2014**, *6*, 548-558.

(25) Munch, R. C.; Janicki, H.; Volker, I.; Rasbach, A.; Hallek, M.; Buning, H.; Buchholz, C. J. Displaying high-affinity ligands on adeno-associated viral vectors enables tumor cell-specific and safe gene transfer. *Mol Ther* **2013**, *21*, 109-118.

(26) Buning, H.; Srivastava, A. Capsid Modifications for Targeting and Improving the Efficacy of AAV Vectors. *Mol Ther Methods Clin Dev* **2019**, *12*, 248-265.

(27) Zhong, L.; Zhao, W.; Wu, J.; Li, B.; Zolotukhin, S.; Govindasamy, L.; Agbandje-McKenna, M.; Srivastava, A. A Dual Role of EGFR Protein Tyrosine Kinase Signaling in Ubiquitination of AAV2 Capsids and Viral Second-strand DNA Synthesis. *Molecular Therapy* **2007**, *15*, 1323-1330.

(28) Maersch, S.; Huber, A.; Buning, H.; Hallek, M.; Perabo, L. Optimization of stealth adeno-associated virus vectors by randomization of immunogenic epitopes. *Virology* **2010**, *397*, 167-175.

(29) Subramanian, S.; Parthasarathy, R.; Sen, S.; Boder, E. T.; Discher, D. E. Species- and cell type-specific interactions between CD47 and human SIRPalpha. *Blood* **2006**, *107*, 2548-2556.

(30) Taro Shimizu, M. I., Yasuo Yoshioka, Tatsuhiro Ishida, Shinsaku Nakagaw, and Hiroshi Kiwadaa. Intravenous Administration of Polyethylene Glycol-Coated (PEGylated) Proteins and PEGylated Adenovirus Elicits an Anti-PEG Immunoglobulin M Response. *Biol. Pharm. Bull.* **2012**, *35*, 1336–1342.

(31) Bartel, M.; Schaffer, D.; Buning, H. Enhancing the Clinical Potential of AAV Vectors by Capsid Engineering to Evade Pre-Existing Immunity. *Front Microbiol* **2011**, *2*, 204.

(32) Jaiswal, S.; Jamieson, C. H.; Pang, W. W.; Park, C. Y.; Chao, M. P.; Majeti, R.; Traver, D.; van Rooijen, N.; Weissman, I. L. CD47 is

upregulated on circulating hematopoietic stem cells and leukemia cells to avoid phagocytosis. *Cell* **2009**, *138*, 271-285.

(33) Bouguermouh, S.; Van, V. Q.; Martel, J.; Gautier, P.; Rubio, M.; Sarfati, M. CD47 Expression on T Cell Is a Self-Control Negative Regulator of Type 1 Immune Response. *The Journal of Immunology* **2008**, *180*, 8073-8082.

(34) Rodriguez, P. L.; Harada, T.; Christian, D. A.; Pantano, D. A.; Tsai, R. K.; Discher, D. E. Minimal "Self" peptides that inhibit phagocytic clearance and enhance delivery of nanoparticles. *Science* **2013**, *339*, 971-975.

(35) Sosale, N. G.; Ivanovska, II; Tsai, R. K.; Swift, J.; Hsu, J. W.; Alvey, C. M.; Zoltick, P. W.; Discher, D. E. "Marker of Self" CD47 on lentiviral vectors decreases macrophage-mediated clearance and increases delivery to SIRPA-expressing lung carcinoma tumors. *Mol Ther Methods Clin Dev* **2016**, *3*, 16080.

(36) Judd, J.; Wei, F.; Nguyen, P. Q.; Tartaglia, L. J.; Agbandje-McKenna, M.; Silberg, J. J.; Suh, J. Random Insertion of mCherry Into VP3 Domain of Adeno-associated Virus Yields Fluorescent Capsids With no Loss of Infectivity. *Mol Ther Nucleic Acids* **2012**, *1*, e54.

(37) Grieger, J. C.; Snowdy, S.; Samulski, R. J. Separate basic region motifs within the adeno-associated virus capsid proteins are essential for infectivity and assembly. *J Virol* **2006**, *80*, 5199-5210.

(38) Anne Girod, C. E. W., Zolta!n Za!dori, Martin Ried, Kristin Leike, Peter Tijssen,; Hallek, J. The VP1 capsid protein of adeno-associated virus

type 2 is carrying a phospholipase A2 domain required for virus infectivity. *Journal of General Virology* (**2002**, 83, 973–978).

(39) Salganik, M.; Aydemir, F.; Nam, H. J.; McKenna, R.; Agbandje-McKenna, M.; Muzyczka, N. Adeno-associated virus capsid proteins may play a role in transcription and second-strand synthesis of recombinant genomes. *J Virol* **2014**, 88, 1071-1079.

(40) Fikret Aydemir, M. S., Justyna Resztak, Jasbir Singh, Antonette Bennett, Mavis Agbandje-McKenna, Nicholas Muzyczkaa. Mutants at the 2-Fold Interface of Adeno-associated Virus Type 2 (AAV2) Structural Proteins Suggest a Role in Viral Transcription for AAV Capsids. *J Virol* **2016**, 90, 7196-7204.

(41) Zhong, L.; Li, B.; Jayandharan, G.; Mah, C. S.; Govindasamy, L.; Agbandje-McKenna, M.; Herzog, R. W.; Weigel-Van Aken, K. A.; Hobbs, J. A.; Zolotukhin, S.; Muzyczka, N.; Srivastava, A. Tyrosine-phosphorylation of AAV2 vectors and its consequences on viral intracellular trafficking and transgene expression. *Virology* **2008**, 381, 194-202.

(42) Zhao, W.; Zhong, L.; Wu, J.; Chen, L.; Qing, K.; Weigel-Kelley, K. A.; Larsen, S. H.; Shou, W.; Warrington, K. H., Jr.; Srivastava, A. Role of cellular FKBP52 protein in intracellular trafficking of recombinant adeno-associated virus 2 vectors. *Virology* **2006**, 353, 283-293.

(43) Aslanidi, G. V.; Rivers, A. E.; Ortiz, L.; Song, L.; Ling, C.; Govindasamy, L.; Van Vliet, K.; Tan, M.; Agbandje-McKenna, M.; Srivastava, A. Optimization of the capsid of recombinant adeno-associated virus 2 (AAV2) vectors: the final threshold? *PLoS One* **2013**, 8, e59142.

(44) Gabriel, N.; Hareendran, S.; Sen, D.; Gadkari, R. A.; Sudha, G.; Selot, R.; Hussain, M.; Dhaksnamoorthy, R.; Samuel, R.; Srinivasan, N.; Srivastava, A.; Jayandharan, G. R. Bioengineering of AAV2 capsid at specific serine, threonine, or lysine residues improves its transduction efficiency in vitro and in vivo. *Hum Gene Ther Methods* **2013**, *24*, 80-93.

(45) Li, B.; Ma, W.; Ling, C.; Van Vliet, K.; Huang, L. Y.; Agbandje-McKenna, M.; Srivastava, A.; Aslanidi, G. V. Site-Directed Mutagenesis of Surface-Exposed Lysine Residues Leads to Improved Transduction by AAV2, But Not AAV8, Vectors in Murine Hepatocytes In Vivo. *Hum Gene Ther Methods* **2015**, *26*, 211-220.

(46) Murray, S.; Nilsson, C. L.; Hare, J. T.; Emmett, M. R.; Korostelev, A.; Ongley, H.; Marshall, A. G.; Chapman, M. S. Characterization of the capsid protein glycosylation of adeno-associated virus type 2 by high-resolution mass spectrometry. *J Virol* **2006**, *80*, 6171-6176.

## Ch. 5 Conclusions and Future Work

In sum, this thesis research shares our deepened understanding of AAV capsid engineering strategies and essential aspects that govern AAV capsid biology. In Chapter 2, I uncovered amino acid characteristics that regulate the function of protease-activatable AAV vectors (Provector). I discovered that Provector function is controlled through both electrostatic interactions and steric obstruction, not primarily electrostatic interactions as previously thought. Furthermore, I found that insertion of positively charged amino acids, K4 and R4, lead to deleterious structural effects. Both viruses form at extremely low titers, but have different trends in genome protection. The K4 capsid does not protect its genome effectively while the R4 capsid is able to protect its genome. Based on these unexpected results, insertion of positively charged amino acids should be carefully considered for genetic engineering of the AAV2 capsid. Through examining amino acid properties, I have provided design rules to continue provector genetic engineering for targeting diseased cells. For clinical application, provectors may be further engineered to treat other diseases characterized as an enzyme-rich environment. For example, other enzymatic biomarkers are upregulated in Alzheimer's disease. Therefore, alternative consensus sequences may be constructed to re-target the provector to neurodegenerative diseased sites.

In Chapter 3, I constructed an immune-evasive AAV vector that evades macrophage uptake. As a feasible strategy, I inserted a stealth self-peptide (SP) in the AAV2 capsid to not be recognized as a 'foreign invader' by macrophages. I

showed that genetic modification of the capsid with SP incorporation does not cause adverse structural or transduction effects. Furthermore, I demonstrated that AAV-SP vectors display decreased phagocytic susceptibility. My promising results highlighted that AAV-SP vectors are promising candidates to improve AAV stealthiness *in vitro*. Further studies using *in vivo* models should be performed to test for therapeutic efficacy of AAV-SP vectors to decrease the humoral immune response, in particular, NAb production upon AAV-SP administration.

In the final chapter, Chapter 4, I shifted my research efforts to understanding AAV intracellular trafficking and infectivity. In exploring regions of the AAV2 VP1/2 N-terminus, we identified amino acids that are essential for transduction. In particular, serine residues of a triplet motif located in positions 155-157, including the flanking residues, D154 and G158 showed importance to be further investigated. Knowing that alanine mutants (D154A, S155A, S155-7A, G158A) cause a dramatic decrease in transduction efficiency, I studied viral intracellular trafficking of these mutants. Surprisingly, I discovered that ineffective nuclear uncoating and transgene transcription defects may hinder their transduction efficiency. As we gain better insights of AAV trafficking, better strategies should become available to optimize transduction efficiency. Additional mechanistic studies on role of capsid phosphorylation, scaffold and chaperone proteins, and viral intracellular processing may provide additional information that can be used to develop improved AAV vectors.